PLOS GENETICS

RESEARCH ARTICLE

Destabilization of chromosome structure by histone H3 lysine 27 methylation

Mareike Möller[1,2], Klaas Schotanus[3], Jessica L. Soyer[4], Janine Haueisen[1,2], Kathrin Happ[1], Maja Stralucke[1], Petra Happel[5], Kristina M. Smith[6], Lanelle R. Connolly[7], Michael Freitag[7], Eva H. Stukenbrock[1,2]*

1 Environmental Genomics, Christian-Albrechts University, Kiel, Germany, **2** Max Planck Fellow Group Environmental Genomics, Max Planck Institute for Evolutionary Biology, Plön, Germany, **3** Department of Molecular Genetics and Microbiology, Duke University Medical Center, Durham, NC, United States of America, **4** UMR BIOGER, INRA, AgroParisTech, Université Paris-Saclay, Thiverval-Grignon, France, **5** Max Planck Institute for Terrestrial Microbiology, Marburg, Germany, **6** Department of Biology, Oregon State University—Cascades, Bend, OR, United States of America, **7** Department of Biochemistry and Biophysics, Oregon State University, Corvallis, OR, United States of America

* estukenbrock@bot.uni-kiel.de

Citation: Möller M, Schotanus K, Soyer JL, Haueisen J, Happ K, Stralucke M, et al. (2019) Destabilization of chromosome structure by histone H3 lysine 27 methylation. PLoS Genet 15 (4): e1008093. https://doi.org/10.1371/journal.pgen.1008093

Editor: Hiten D. Madhani, University of California San Francisco, UNITED STATES

Received: November 10, 2018

Accepted: March 15, 2019

Published: April 22, 2019

Data Availability Statement: Sequencing raw reads (FASTQ files) of all genomic, ChIP-seq and RNA-seq data are available online at Sequence Read Archive (SRA) under BioProject ID PRJNA494102.

Funding: Research in the lab of EHS on histone modifications in Zymoseptoria tritici is funded by a fellowship from the Max Planck Society to EHS. Work on H3 lysine 27 methylation in the lab of MF was supported by NSF grants (MCB 1515998 and MCB1818006).The funders had no role in study

Abstract

Chromosome and genome stability are important for normal cell function as instability often correlates with disease and dysfunction of DNA repair mechanisms. Many organisms maintain supernumerary or accessory chromosomes that deviate from standard chromosomes. The pathogenic fungus *Zymoseptoria tritici* has as many as eight accessory chromosomes, which are highly unstable during meiosis and mitosis, transcriptionally repressed, show enrichment of repetitive elements, and enrichment with heterochromatic histone methylation marks, e.g., trimethylation of H3 lysine 9 or lysine 27 (H3K9me3, H3K27me3). To elucidate the role of heterochromatin on genome stability in *Z. tritici*, we deleted the genes encoding the methyltransferases responsible for H3K9me3 and H3K27me3, *kmt1* and *kmt6*, respectively, and generated a double mutant. We combined experimental evolution and genomic analyses to determine the impact of these deletions on chromosome and genome stability, both *in vitro* and *in planta*. We used whole genome sequencing, ChIP-seq, and RNA-seq to compare changes in genome and chromatin structure, and differences in gene expression between mutant and wildtype strains. Analyses of genome and ChIP-seq data in H3K9me3-deficient strains revealed dramatic chromatin reorganization, where H3K27me3 is mostly relocalized into regions that are enriched with H3K9me3 in wild type. Many genome rearrangements and formation of new chromosomes were found in the absence of H3K9me3, accompanied by activation of transposable elements. In stark contrast, loss of H3K27me3 actually increased the stability of accessory chromosomes under normal growth conditions *in vitro*, even without large scale changes in gene activity. We conclude that H3K9me3 is important for the maintenance of genome stability because it disallows H3K27me3 in regions considered constitutive heterochromatin. In this system, H3K27me3 reduces the overall stability of accessory chromosomes, generating a "metastable" state for these quasi-essential regions of the genome.

design, data collection and analysis, decision to publish, or preparation of the manuscript.

Competing interests: The authors have declared that no competing interests exist.

Author summary

Genome and chromosome stability are essential to maintain normal cell function and viability. However, differences in genome and chromosome structure are frequently found in organisms that undergo rapid adaptation to changing environmental conditions, and in humans are often found in cancer cells. We study genome instability in a fungal pathogen that exhibits a high degree of genetic diversity. Regions that show extraordinary diversity in this pathogen are the transposon-rich accessory chromosomes, which contain few genes that are of unknown benefit to the organism but maintained in the population and thus considered "quasi-essential". Accessory chromosomes in all fungi studied so far are enriched with markers for heterochromatin, namely trimethylation of H3 lysine 9 and 27 (H3K9me3, H3K27me3). We show that loss of these heterochromatin marks has strong but opposing effects on genome stability. While loss of the transposon-associated mark H3K9me3 destabilizes the entire genome, presence of H3K27me3 favors instability of accessory chromosomes. Our study provides insight into the relationship between chromatin and genome stability and why some regions are more susceptible to genetic diversity than others.

Introduction

Chromatin structure plays an important role in genome organization and gene expression [1–3]. A well-studied hallmark of epigenetic regulation is the reversible modification of histone tails, which can alter chromatin structure [4]. Chromatin structure determines accessibility of the underlying DNA to regulatory elements, whereby tightly packed DNA, known as heterochromatin, is less accessible for DNA binding proteins and usually shows little transcriptional activity [5]. Heterochromatic regions often cluster together and are spatially separated from more transcriptionally active and accessible euchromatic regions [6]. Specific histone modifications are associated with either heterochromatic or euchromatic regions. Some of the most studied histone modifications are histone H3 lysine 9 di- or trimethylation (H3K9me2/3) and H3K27me2/3 as markers for heterochromatin and H3K4me2/3 as markers for euchromatin [7].

H3K9me2/3 is catalyzed by the histone methyltransferase KMT1 (Su[var]3–9) [8,9], in fungi also called Clr4 [10] or DIM-5 [11]. Previous studies demonstrated enrichment of this constitutive heterochromatin mark in repeat-rich regions and a clear link with the control of transposable elements (TE) and genome stability [12–14]. For example, H3K9 methylation has been shown to be involved in suppression of meiotic recombination in *Arabidopsis thaliana* [15] and the control of DNA methylation in *Neurospora crassa* [11].

H3K27me2/3, usually associated with "facultative heterochromatin", is catalyzed by KMT6 (E[Z]) as part of the PRC2 complex [16]. In plants, fungi, and animals, this histone mark is used to generate "transcriptional memory" and is easily reversible when environmental or endogenous stimuli require organismal responses. In many organisms, H3K27 methylation is required for development and cell differentiation [17–23], and aberrant H3K7me3 distribution is prevalent in cancer cells [24–26]. In fungi, H3K27me3 correlates with subtelomeric gene silencing [22,23,27], and has been shown to play a role in development, pathogenicity, and transcriptional regulation of secondary metabolite gene clusters [21,28,29].

H3K27me3 is also a hallmark of accessory chromosomes, which are found in several fungal plant pathogens [28,30,31]. Accessory chromosomes are not essential for survival under all

environmental conditions, and thus encode "quasi-essential" genes [32] that can confer selective advantages under some conditions e.g. in a specific host species, resulting in presence or absence of these chromosomes among specific individuals of a given species. They are also characterized by extensive structural rearrangements and length variation [33,34]. In some species (*Fusarium oxysporum*, *Nectria haematococca*, *Alternaria alternata*), accessory chromosomes increase virulence [35–38]. However, in the wheat pathogen *Zymoseptoria tritici*, some accessory chromosomes have been demonstrated to confer reduced fitness and virulence *in planta* [39], suggesting that there are other stages in the life cycle when they become important. Accessory chromosomes of fungi differ structurally from core chromosomes by higher repeat and lower gene density compared to core chromosomes and show little transcriptional activity [35,40–43]. Transcriptional silencing can be explained by their predominantly heterochromatic structure, with H3K27me3 enrichment on almost the entire chromosome and H3K9me3 covering repetitive sequences [28,30]. Centromeres and telomeres are important structural components of chromosomes. In plants, centromeres of B chromosomes, equivalents to fungal accessory chromosomes, differ from those of A chromosomes [44], but in *Z. tritici* centromeres, telomere repeats, and subtelomeric regions are so far by all measures near identical on core and accessory chromosomes [31]. Though accessory chromosomes are a frequent phenomenon in fungi, little is known about their origin and maintenance. Studies on chromosome stability revealed that accessory chromosomes are highly unstable, both during mitosis [36,45,46] and meiosis [47].

Here, we investigated to what extent the particular histone methylation pattern on accessory chromosomes contributes to the structural differences, transcriptional repression and instability. We shed light on the roles of H3K9me3 and H3K27me3 on genome stability in the hemi-biotrophic wheat pathogen *Z. tritici* that reproduces both asexually and sexually. By combining experimental evolution with genome, transcriptome and ChIP sequencing, we show that both heterochromatin-associated histone methylation marks contribute significantly, but in distinct ways, to chromosome stability and integrity. While the presence of H3K27me3 enhances chromosome loss and instability, loss of H3K9me3 promotes chromosome breakage, segmental duplications as well as the formation of new chromosomes – possibly resembling the emergence of accessory chromosomes. Taken together, our findings demonstrate the importance of constitutive heterochromatin for maintaining genome stability and gene silencing as well as an unexpected destabilizing influence of facultative heterochromatin on mitotic accessory chromosome transmission. The presence of eight accessory chromosomes in the reference isolate IPO323 makes *Z. tritici* an excellent model to study accessory chromosome characteristics and dynamics, which relates to general interest in chromosome maintenance in cancer or other aneuploid cell types.

Results

Deletion of histone methyltransferase encoding genes *kmt1* and *kmt6* in *Zymoseptoria tritici*

To investigate the impact of heterochromatin on fitness, transcription and genome stability in *Z. tritici*, we generated mutants of two histone methyltransferases Kmt1 (*S. pombe* Clr4; *N. crassa* DIM-5, *Fusarium* KMT1, *H. sapiens* SUV39H1) and Kmt6 (*N. crassa* SET-7; *Fusarium* KMT6; *H. sapiens* EZH2). We identified the *Z. tritici* genes by BLAST searches with the *N. crassa* and *F. graminearum* protein coding sequences as baits. Kmt1 is encoded by *kmt1* (Zt_chr_1_01919), and Kmt6 is encoded by *kmt6* (Zt_chr_4_00551) [48]. We used *Agrobacterium tumefaciens*-mediated transformation [49] to delete both genes in a derivate of the *Z. tritici* reference isolate IPO323 that lost chromosome 18 during *in vitro* growth, here called Zt09

[31,40,41]. Correct integration of the *hph* gene, which confers hygromycin resistance [49], and *kmt1* or *kmt6* deletion were verified by PCR and Southern analyses (S1 and S2 Figs). We generated a double deletion mutant by deleting the *kmt1* gene in a *kmt6* deletion mutant background by using resistance to nourseothricin conferred by the *nat* gene [50] as an additional selection marker. We isolated several independent transformants, including eight *Δkmt1*, six *Δkmt6* and ten *Δkmt1 Δkmt6* double mutants (from here on abbreviated *Δk1/k6*). For further studies we selected two or three mutants of each type (S1 Table). *Δkmt1* and *Δkmt6* single mutants were complemented by re-integrating the previously deleted gene and a neo^+ resistance marker that can confer G418 resistance at the native gene loci (S2 Fig).

We performed ChIP-seq on Zt09, *Δkmt1* (Zt125-#68, -#80), *Δkmt6* (Zt110-#283, -#285, -#365) and the double deletion mutant *Δk1/k6* (Zt219-#23, -#116), which verified the absence of H3K9me3 in *Δkmt1* and *Δk1/k6*, and the absence of H3K27me3 in *Δkmt6* and *Δk1/k6* mutants (S3 Fig), confirming that Kmt1 and Kmt6 are the only histone methyltransferases in *Z. tritici* responsible for H3K9 and H3K27 trimethylation, respectively. An overview of the subsequent experiments and key results are summarized in S1 Fig.

Deletion of *kmt1*, but not *kmt6*, severely impacts *in vitro* and *in planta* growth

To assess if deletion of *kmt1* and *kmt6* has an impact on *in vitro* growth or pathogenicity on wheat, we performed comparative growth and virulence assays comparing the mutants to the wild type Zt09. To compare growth rates, the reference strain Zt09, deletion and complemented strains were grown in liquid YMS cultures and the OD_{600} was measured until cells reached stationary phase. Overall, the Δ*kmt1* strains and Δ*k1/k6* double deletion mutants showed significantly reduced growth *in vitro* (S4 Fig). The Δ*kmt6* mutants and both $kmt1^+$ and $kmt6^+$ complementation strains showed no significant differences in growth compared to Zt09 (Wilcoxon rank-sum test, *p*-values: Δ*kmt1* 0.025; Δ*kmt6* 0.42; Δ*k1/k6* 0.005; $kmt1^+$ 0.28; $kmt6^+$ 0.63).

We furthermore assessed the tolerance of the Δ*kmt1*, Δ*kmt6* and Δ*k1/k6* mutants to abiotic stress *in vitro* by testing temperature, cell wall, oxidative, and genotoxic stressors. As observed in the growth assays, the Δ*kmt1* and Δ*k1/k6* double deletion mutants showed overall reduced growth under all tested conditions (S5 Fig), especially under osmotic stress induced by high sorbitol concentrations. The Δ*kmt6* mutants showed little differences compared to Zt09; however, elevated temperatures often, but not always, led to increased melanization in the Δ*kmt6* mutants suggesting involvement of H3K27me3 in the response to temperature stress. This phenotype was reversed in the complemented $kmt6^+$ strain (S6 Fig).

To study the effect of the histone methyltransferase deletions on the ability to infect wheat (*Triticum aestivum*), we inoculated leaves of the susceptible cultivar Obelisk with single cell cultures of Δ*kmt1*, Δ*kmt6*, the Δ*k1/k6* double deletion mutant and Zt09. The infection assays demonstrated significant impact of both H3K27me3 and H3K9me3 on virulence. While the number of pycnidia and necrotic leaf areas only decreased in the Δ*kmt6* mutants, wheat infection by Δ*kmt1* and Δ*k1/k6* mutants resulted in almost no symptoms (S7 Fig). If any symptoms developed, these appeared considerably later than symptoms caused by the reference Zt09 and the Δ*kmt6* mutants (S7 Fig).

Loss of H3K9me3 allows H3K27me3 to invade repeat-rich regions

We next addressed how the deletion of *kmt1* and *kmt6* impacts the distribution of three histone modifications (H3K4me2, H3K9me3, H3K27me3) by ChIP-seq (S2 Table). We previously found that H3K4me2 is associated with gene-rich, transcriptionally active regions on

core chromosomes, that constitutive heterochromatin, enriched with H3K9me3, forms almost exclusively on repetitive elements, and that facultative heterochromatin, enriched with H3K27me3, forms nearly on the entire length of all accessory chromosomes and the subtelomeric regions of core chromosomes [31] (Fig 1).

We computed the sequence coverage of each histone modification per chromosome to estimate the global effects on chromatin structure. The absence of one histone methylation mark had differential effects on the distribution of the other two methylation marks on core and accessory chromosomes (Fig 1, Table 1). In the Δ*kmt1* mutants, the amount of sequences enriched with H3K27me3 decreases on the accessory chromosomes when compared to Zt09, representing the opposite trend to the observations made on the core chromosomes, where we observed an increased amount of sequences enriched in H3K27me3 (Fig 1, Table 1). However, this effect varies on different accessory chromosomes (Table 1, Fig 2). The difference in H3K27me3 distribution can be explained by relocation of H3K27me3 to former H3K9me3-associated sequences in the *Δkmt1* mutant (Fig 1). While fewer genes are associated with H3K27me3 (Fig 2), more TEs show H3K27me3 enrichment in the Δ*kmt1* mutant (Fig 2) compared to Zt09. These observations reveal that loss of H3K9me3 promotes H3K27me3 relocation to TEs and confers simultaneous loss of H3K27me3 at positions with this histone mark in the reference strain. The subtelomeric H3K27me3 enrichment, however, is not affected by this relocation, which explains why we observe opposite effects on core and accessory chromosomes, as core chromosomes predominantly show H3K27me3 enrichment in subtelomeric regions while accessory chromosomes show overall enrichment with H3K27me3. H3K4me2 increases on both core and accessory chromosomes, with accessory chromosomes showing a considerably higher relative increase compared to H3K4me2 in Zt09 (Table 1).

Conversely, H3K9me3 is not affected by loss of H3K27me3 in the Δ*kmt6* mutants, and we did not detect relocation of H3K9me3 as well as only minor differences in coverage. H3K4me2 enrichment does increase on accessory chromosomes, but not to the same extent as observed in the Δ*kmt*1 mutants and it slightly decreases on core chromosomes (Table 1), suggesting minor effects of *Δkmt6* on transcriptional activation. In the Δ*k1/k6* double deletion mutants, where both H3K9me3 and H3K27me3 are not present, we detected an increase in H3K4me2, similar to the Δ*kmt*1 single mutants on core chromosomes and slightly higher on the accessory chromosomes.

In summary, loss of H3K9me3 has a great impact on H3K27me3 distribution, while loss of H3K27me3 has little influence on H3K9me3. Deletion of *kmt1* promotes large scale relocalization of other histone modifications, suggesting more dramatic effects on genome organization and transcriptional activation than deletion of *kmt6*.

H3K27me3 has little effects on transcriptional activation, while loss of H3K9me3 enhances activation of TEs

In other species, H3K27me3 plays a crucial role in gene regulation, while H3K9me3 is involved in silencing of TEs [13,21,28]. Based on our observations from ChIP-seq data, we hypothesized that the two histone methylation marks have similar effects in *Z. tritici*. To test this hypothesis directly, we sequenced transcriptomes of two biological replicates of Zt09 and two independent transformants of the Δ*kmt1*, Δ*kmt6*, and Δ*k1/k6* deletion mutants after *in vitro* growth for 2 days representing exponential growth (S2 Table).

First, we compared the total number of expressed genes. In total, 11,839 genes are annotated in the reference isolate [48]. Out of these, 8,906 are expressed (RPKM >2) in Zt09 during *in vitro* growth. The number of expressed genes is higher in both the Δ*kmt1* (9,259) and the Δ*k1/k6* (9,459) mutants, but to our surprise, lower in the Δ*kmt6* (8,717) mutants (Fig 3A, S3

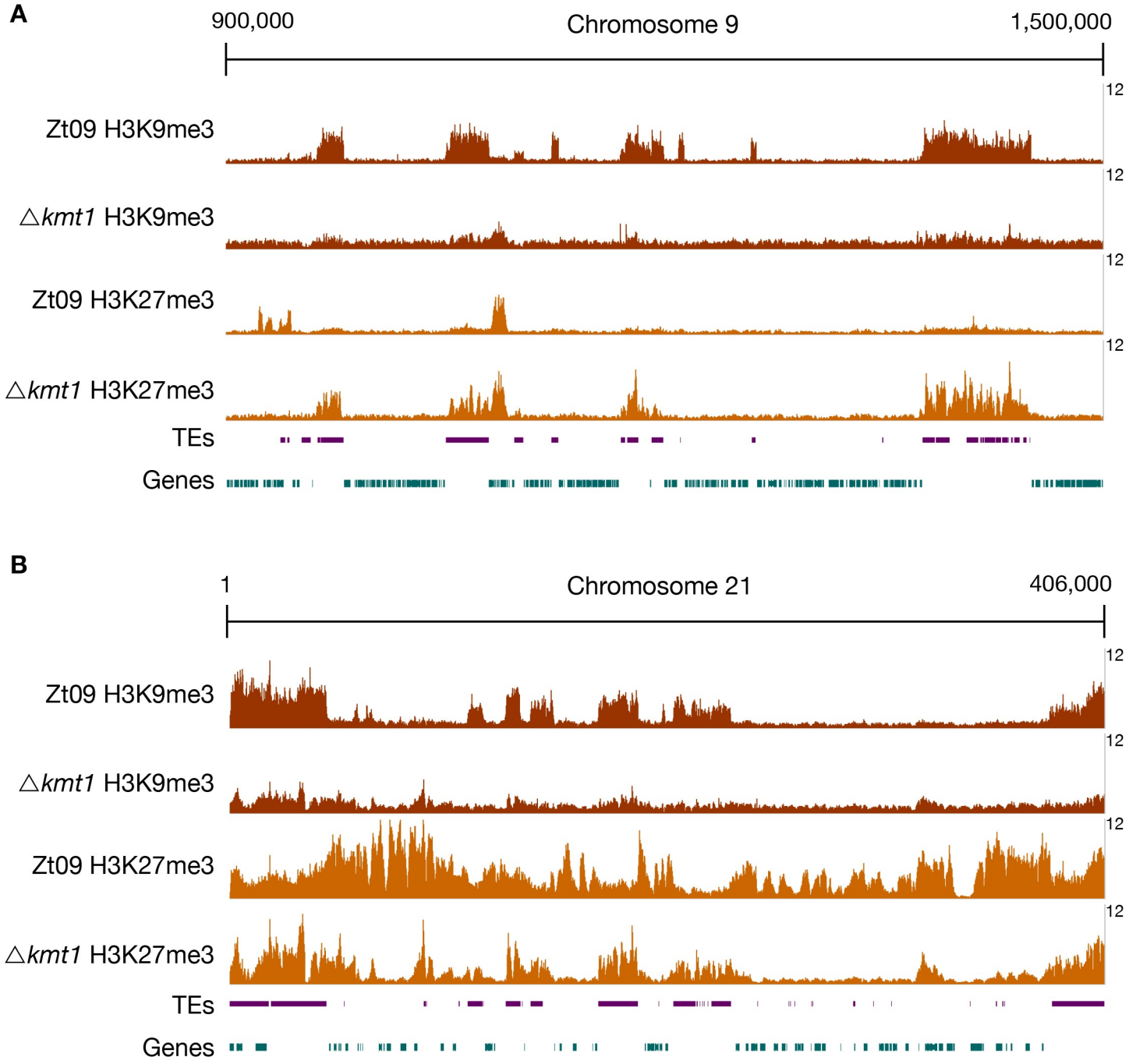

Fig 1. ChIP-seq reveals relocation of H3K27me3 on core (A) and accessory (B) chromosomes in Δ*kmt1* mutants. By analyzing ChIP-seq data in the Δ*kmt1* mutants we found that enrichment of H3K27me3 moves to sequences that are normally enriched with H3K9me3. A region on core chromosome 9 **(A)** is shown, where H3K27me3 is strongly enriched at former H3K9me3 regions, but depleted from its original positions. On accessory chromosomes **(B)**, here full-length chromosome 21 as an example, there are similar dynamics as observed on core chromosomes. Accessory chromosomes normally show overall enrichment of H3K27me3. In absence of H3K9me3, H3K27me3 concentrates on former H3K9me3 regions, again being depleted from its original position. However, this effect varies between accessory chromosomes (Fig 2). The low amount of background found in Δ*kmt1* is due to the repetitive nature of the H3K9me3-enriched regions. All shown ChIP-seq tracks are normalized to 1x coverage (coverage indicated on the right) [107].

https://doi.org/10.1371/journal.pgen.1008093.g001

Table 1. Percentage of sequence coverage (significantly enriched regions) of core and accessory chromosomes with H3K4me2, H3K9me3 and H3K27me3 relative to the chromosome length. Minimum and maximum values refer to the chromosomes showing highest or lowest sequence coverage with enrichment of the respective histone modification. H3K4me2 coverage on accessory chromosomes increases in all mutant strains, while there are little differences in the overall coverage with H3K9me3 between Zt09 and *Δkmt6*. H3K27me3 enrichment increases on core chromosomes and decreases on accessory chromosomes in the *Δkmt1* mutant.

		Core			Accessory		
	Modification	**mean**	**Min**	**max**	**mean**	**min**	**max**
Zt09	H3K4me2	23.99	17.76	31.26	5.03	1.19	9.44
△*kmt1*	H3K4me2	25.25	18.51	32.78	9.68	5.67	17.32
△*kmt6*	H3K4me2	22.74	16.83	29.54	6.22	3.32	10.97
△*k1/k6*	H3K4me2	25.39	19.11	32.69	12.28	8.47	19.96
Zt09	H3K9me3	20.14	10.84	28.71	41.03	30.78	55.97
△*kmt6*	H3K9me3	20.30	11.24	28.27	36.59	26.71	55.74
Zt09	H3K27me3	9.74	3.74	31.72	92.53	67.07	99.20
△*kmt1*	H3K27me3	14.99	6.08	32.77	77.55	56.44	96.82

https://doi.org/10.1371/journal.pgen.1008093.t001

Table). This is in contrast to previous studies, where deletion of *kmt6* resulted in activation of otherwise silenced gene clusters and overall transcriptional activation [21,23,27,28]. We focused on differential gene expression between core and accessory chromosomes because genes on accessory chromosomes are silent under most conditions that have been tested. While 80% of genes on core chromosomes are expressed in Zt09, only ~25% of genes located on accessory chromosomes display transcriptional activity. Transcription of genes on accessory chromosomes is higher in all mutant strains, ~40–50% (Fig 3A, S3 Table), revealing gene activation on accessory chromosomes specifically upon removal of H3K27me3 or H3K9me3.

We further explored patterns of differential gene expression. Genome wide, 1,365 predicted genes were associated with H3K27me3 and 258 genes with H3K9me3 in Zt09 and the vast majority of these genes shows little transcriptional activity. Interestingly, only a small fraction of genes associated with these histone marks were activated or differentially expressed in the mutants (S4 Table). This indicates that loss of any of these methylation marks is not sufficient for transcriptional activation suggesting additional mechanisms involved in the transcriptional regulation of these genes.

In other fungi, removal of H3K9me3 and especially H3K27me3 was linked to the activation of certain gene classes, in particular secondary metabolite gene clusters [21,28,29]. To assess if genes with a specific function are enriched amongst the activated genes, we performed Gene Ontology (GO) enrichment analysis (topGO, Fisher's exact test, p-value < 0.01). Consistent with the higher total number of expressed genes, we found the majority of differentially expressed (DE) genes (DESeq2, $P_{adj} < 0.001$, log2 fold-change > 2) to be significantly upregulated in the Δ*kmt1* mutant (365 of 477) and in the Δ*k1/k6* mutant (368 of 477), whereas a majority of DE genes was downregulated in the Δ*kmt6* mutant (188 of 310) (S5 Table).

We found two GO categories enriched amongst upregulated genes in Δ*kmt1* and Δ*k1/k6* mutants: DNA integration (GO:0015074) and RNA-dependent DNA replication (GO:0006278). Predicted functions assessed by BLAST analyses of the proteins encoded by the upregulated genes in these categories include reverse transcriptases, integrases, recombinases and genes containing transposon- or virus-related domains (S6 Table). Consistent with these findings, we detected an increased number of transcripts originating from annotated TEs in the Δ*kmt1* and Δ*k1/k6* mutants, but not in Δ*kmt6* mutants (Fig 3B). This is in agreement with the strong association of TEs with H3K9me3 [31]. Transposons in subtelomeric regions and on accessory chromosomes show additional H3K27me3 enrichment. Removal of H3K9me3, but not of H3K27me3, appears to be responsible for transposon activation but transcription is

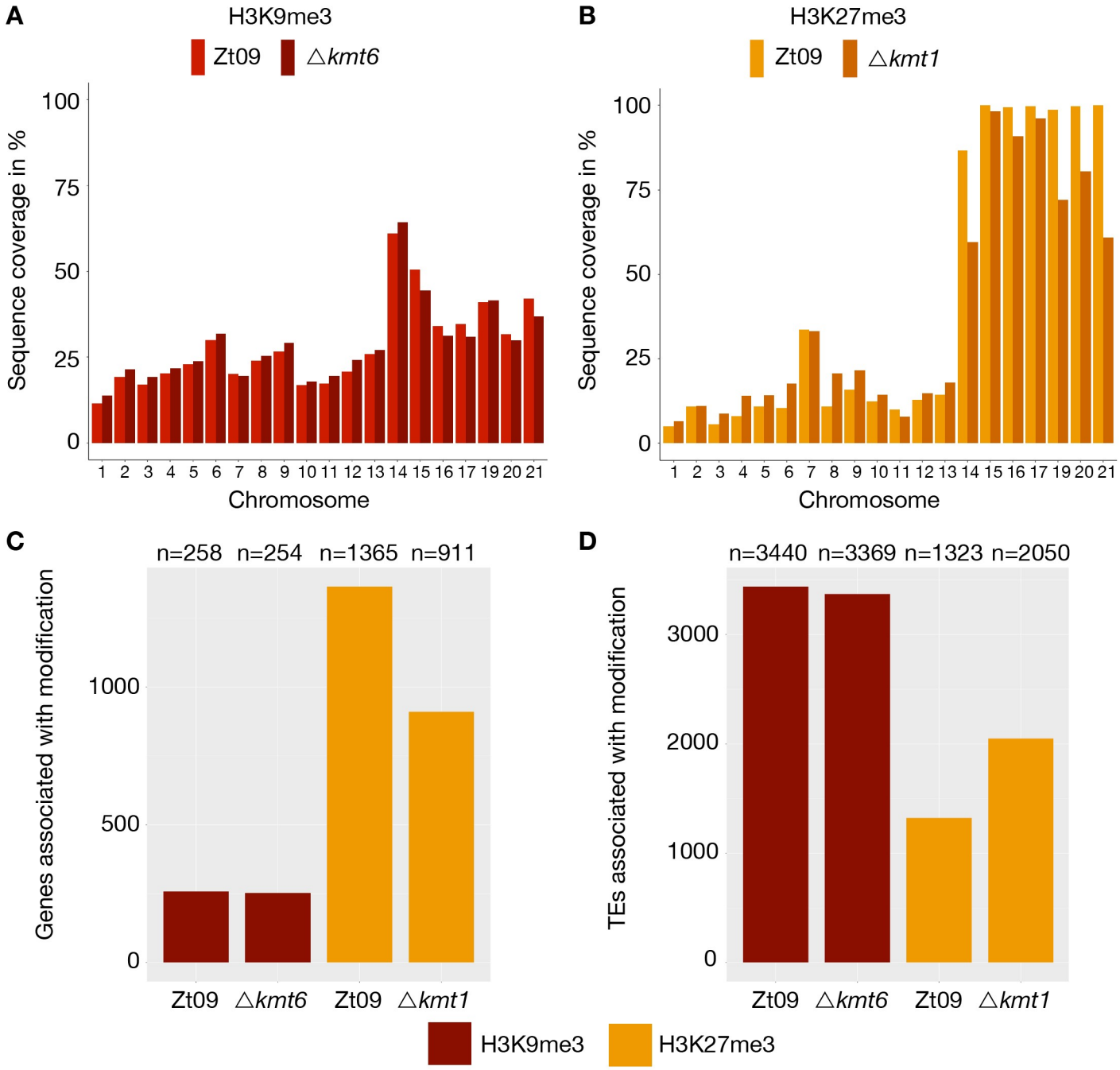

Fig 2. Genome-wide distribution of H3K9me3 and H3K27me3 in Zt09 and mutants. (A) and **(B)** display the percentage of sequence coverage of core and accessory chromosomes with H3K9me3 and H3K27me3 relative to the chromosome length. While there were little differences in the overall coverage with H3K9me3 between Zt09 and Δ*kmt6* (A), H3K27me3 enrichment was increased on core chromosomes and decreased on accessory chromosomes in the Δ*kmt1* mutant (B). Chromosome 7 displayed a higher H3K27me3 coverage compared to the other core chromosomes as the right arm showed characteristics of an accessory chromosome [31]. **(C and D)** Genes (C) and TEs (D) associated with H3K9me3 or H3K27me3 in Zt09 and mutant strains. While there was almost no difference in terms of H3K9me3-associated genes or TEs in the Δ*kmt6* mutants, H3K27me3 relocated from genes to TEs in the Δ*kmt1* mutants.

https://doi.org/10.1371/journal.pgen.1008093.g002

further enhanced when both, H3K27me3 and H3K9me3 are removed in the *Δk1/k6* mutant (Fig 3B; S7 Table).

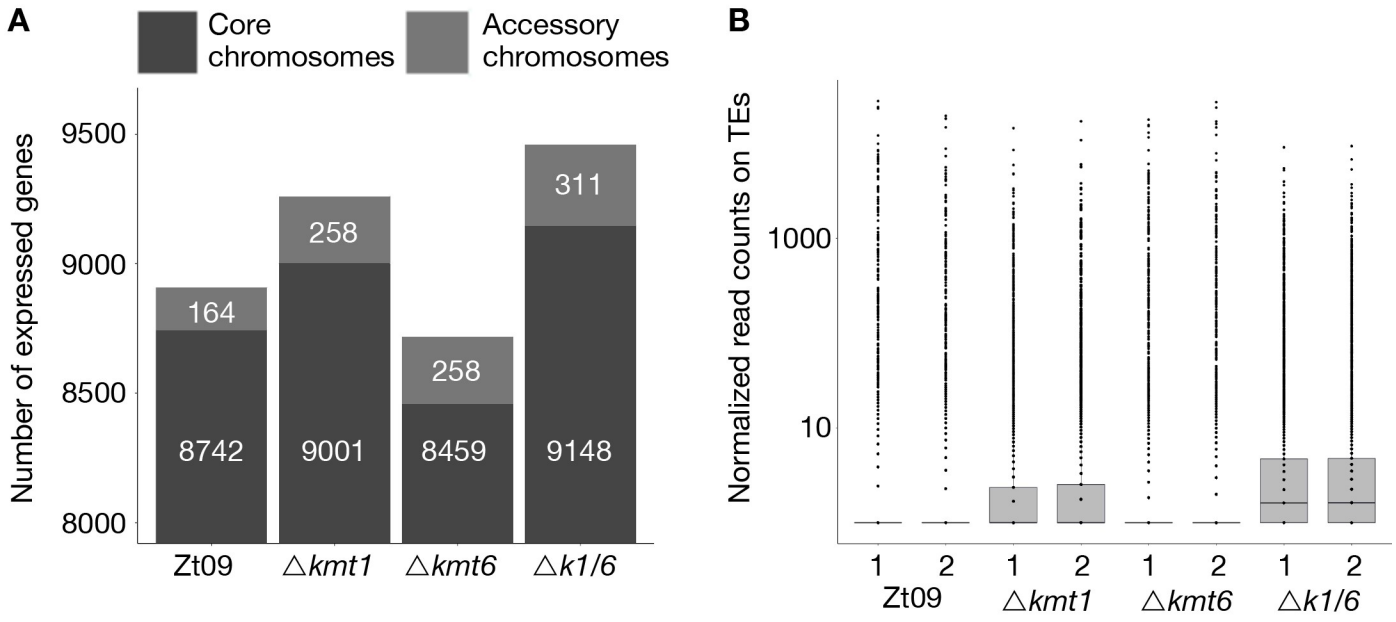

Fig 3. Gene (A) and transposon (B) expression increases in absence of H3K9me3, while loss of H3K27me3 alone decreases the number of expressed genes and does not impact transposon activity. (A) We compared the number of expressed genes in Zt09 and mutant strains. While in all mutants the number of expressed genes increased on accessory chromosomes, surprisingly loss of H3K27me3 alone in the Δ*kmt6* mutants resulted in a reduction of genes expressed on core chromosomes and only a small increase in numbers of genes expressed on accessory chromosomes. **(B)** Loss of H3K9me3, but not H3K27me3 alone, increased the number of transcripts originating from TEs. In absence of both marks (Δ*k1/k6*), the number further increased, likely because H3K27me3 moves to TEs in the Δ*kmt1* single mutant, facilitating silencing.

https://doi.org/10.1371/journal.pgen.1008093.g003

Amongst the genes upregulated in the Δ*kmt6* mutant no GO categories were enriched but based on the previous finding of secondary metabolite activation, we further investigated possible roles of H3K9me3 and H3K27me3 in secondary metabolite gene regulation. Therefore, we identified putative secondary metabolite clusters in the *Z. tritici* reference genome using antiSMASH (antibiotics & Secondary Metabolite Analysis SHell) [51]. We found a total of 27 secondary metabolite clusters, all located on core chromosomes, and merged the identified genes with the existing gene annotation (S8 Table). Except for the activation of one putative cluster on chromosome 7 in the Δ*k1/k6* mutant, we did not identify any differential expression of genes in secondary metabolite clusters. Based on these findings, we conclude that, unlike in other fungi [21,29], H3K9me3 and H3K27me3 are not involved in transcriptional regulation of secondary metabolites in *Z. tritici* under the tested conditions.

Taken together, removal of these histone modifications has little consequences for the expression of the vast majority of associated genes. As expected from its localization, loss of H3K9me3 increases expression of TEs while absence of H3K27me3 by itself has very little impact on transcriptional activation, thus suggesting that in this organism H3K27me3 does not delineate stereotypical "facultative heterochromatin" as removal of H3K27me3 does not activate gene expression.

Loss of H3K27me3 drastically reduces the loss of accessory chromosomes

Chromosome landmarks, namely centromeric and pericentric regions, telomere repeats and subtelomeric regions are similar on core and accessory chromosomes in *Z. tritici* [31]. Accessory chromosomes are enriched with TEs but share the same TE families as core chromosomes [48]. Nevertheless, accessory chromosomes of *Z. tritici* are highly unstable, both during

Table 2. Chromosome loss rates and frequency of individual accessory chromosome losses in the Zt09[1] reference strain and mutants during short-term evolution experiments. Three replicate cultures were tested per strain.

Chromosome	Zt09	Δ*kmt1*	Δ*kmt6*	Δ*k1/k6*	*kmt1*$^+$	*kmt6*$^+$
14	18	26	2	13	6	10
15	8	0	0	0	6	7
16	9	2	0	2	0	2
17	0	0	5	0	0	0
19	0	0	0	3	0	0
20	2	51	2	17	2	0
21	1	6	1	6	0	0
total loss	38	85	10	41	14	19
total tested	576	576	576	576	288	288
loss rate (%)	6.6	14.8	1.7	7.1	4.88	6.94

[1] Strain Zt09 had previously spontaneously lost chromosome 18 [41].

https://doi.org/10.1371/journal.pgen.1008093.t002

meiosis and vegetative growth *in vitro* and *in planta* [46,47]. The most striking feature that sets these chromosomes apart is almost chromosome-wide enrichment with H3K27me3 and, as a consequence of the higher TE content, increased enrichment with H3K9me3 [31]. To test whether loss of these modifications affects genome and chromosome stability in *Z. tritici*, we conducted two different long-term growth or "lab evolution" experiments to study genome stability and to detect dynamics of accessory chromosome losses in strains deficient for two important chromatin marks (S8 Fig).

To assess whether the specific histone methylation pattern on accessory chromosomes contributes to instability of accessory chromosomes, we performed a short-term *in vitro* growth experiment over four weeks, representing ~80 asexual generations. Zt09, Δ*kmt6*, Δ*kmt1* and a Δ*k1/k6* double deletion mutant, as well as the complemented strains *kmt1*$^+$ and *kmt6*$^+$ were used as progenitors in the experiment. The presence of all accessory chromosomes in the progenitor strains was verified by PCR at the beginning of the experiment. Each strain was grown in three replicate cultures and ~4% of the cell population was transferred to fresh medium every three to four days. After four weeks of growth, we plated dilutions of each culture to obtain single colonies that were subsequently screened by a PCR assay for the presence of accessory chromosomes (Table 2).

Previously, we showed that accessory chromosomes are lost at a rate of ~7% in Zt09 and we documented that accessory chromosomes 14, 15 and 16 are more frequently lost than others [46]. Here we demonstrate that, in comparison to Zt09, the Δ*kmt1* mutant showed a significantly increased chromosome loss rate (one sided Fisher's exact test for count data, p-value = 2.7×10^{-6}). Interestingly, this was not due to an overall increase of accessory chromosome loss, but rather by the dramatically increased (Fisher's exact test, p-value = 3.7×10^{-9}) frequency of loss for chromosome 20 (Table 2). The chromosome loss rate of the other accessory chromosomes was either comparable to Zt09 (Chr. 14, 17, 19, 21) or even significantly lower (Chr. 15 and 16, Fisher's exact test, p-values = 1.2×10^{-3} and 2.5×10^{-5}). This suggests a special role of H3K9me3 for the maintenance of chromosome 20.

In contrast to the Δ*kmt1* mutants, we detected significantly fewer chromosome losses (Fisher's exact test, p-value = 1.2×10^{-4}) in the Δ*kmt6* mutants. Out of 576 tested colonies, only ten had lost an accessory chromosome. This represents a four times lower chromosome loss rate compared to wild type. Therefore, absence of H3K27me3 appears to promote stability of accessory chromosomes. Interestingly, chromosome 17 was lost with the highest frequency in this mutant (5/10) but was not lost in any of the other mutant strains or in the wild type.

The double deletion mutant displayed a similar chromosome loss rate as wild type but showed a chromosome loss distribution comparable to the Δ*kmt1* deletion strain with chromosome 20 being lost significantly more often (Fisher's exact test, *p*-value = 1.23 10^{-4}), and chromosomes 15 and 16 lost less frequently (Fisher's exact test, *p*-values = 1.95 x 10^{-3} and 9 x 10^{-3}, respectively). This suggests that the increase in chromosome stability in Δ*k1/k6* compared to Δ*kmt1* is due to the removal of the destabilizing H3K27me3.

We considered possible reasons for the high rates of loss of chromosome 20 in Δ*kmt1* and Δ*k1/k6* mutant strains by a detailed analysis of TE content, genes and histone methylation redistribution on this chromosome. The proportion of TEs on chromosome 20 is ~23% and thereby considerably lower than the average across the eight accessory chromosomes (33.6% TE content). Consistent with patterns found on the other accessory chromosomes we find no enrichment of specific TE families [48]. Out of the 91 genes on chromosome 20, none has known or even predicted functions; it is therefore difficult to correlate potential gene functions of any of these genes to the enhanced loss rate. Chromosome 20 is one of the chromosomes that exhibits the highest extent of H3K27me3 redistribution (Fig 2) and loss of H3K27me3 in the Δ*k1/k6* double mutant decreases the high loss rate. However, chromosome 20 is still lost at a higher rate in Δ*k1/k6* compared to Zt09, indicating that other, so far unknown, factors are involved in this instability. Moreover, not all accessory chromosomes that exhibit H3K27me3 redistribution (19 and 21) are lost at higher rates, and not all accessory chromosomes are lost at the same rate in the Zt09 wild type, despite being enriched with H3K27me3, further suggesting that additional mechanisms are involved in the instability of chromosome 20.

Both complemented strains, *kmt1*$^{+}$ and *kmt6*$^{+}$, showed chromosome loss rates similar to the wild type strain Zt09 and the highest loss rates for the largest accessory chromosomes (Table 2). This strongly suggests that indeed the absence of the two histone methyltransferases and the respective histone marks influence accessory chromosome dynamics.

In summary, we found that loss of H3K27me3 increases accessory chromosome stability, suggesting a mechanistic explanation for how the widespread H3K27me3 enrichment on accessory chromosomes in normal cells contributes to the previously observed extraordinary chromosome instability.

Loss of H3K9me3 promotes large-scale structural rearrangements mediated by TE instability and redistribution of H3K27me3

In a second evolution experiment, we addressed overall genome stability over a longer period of mitotic growth. The single mutants (Δ*kmt1* and Δ*kmt6*) and Zt09 were grown in triplicate cultures for ~6 months, representing ~500 asexual generations. We sequenced full genomes of progenitors and the evolved populations after 50 transfers to identify structural variations that arose during the experiment. All strains were sequenced to ~100x coverage by Illumina sequencing, and paired-end reads were mapped to the reference genome of IPO323 and normalized to 1x coverage for visualization [40].

We focused our analysis on large scale chromosomal rearrangements such as duplications, deletions, and translocations. Structural variation was detected computationally from sequence alignments, validated experimentally by PFGE and Southern blotting, and additional rearrangements were identified by manual screening of mapped reads. Analysis of progenitor genomes revealed, except for the already known absence of chromosome 18 [41] and the previously described variations (point mutations and short indels) in Zt09 compared to the IPO323 reference genome [46], lower sequence coverage (~0.6x) on chromosome 17 in the Δ*kmt6* progenitor strain (Fig 4A). This difference can only be explained by a lower copy number in the

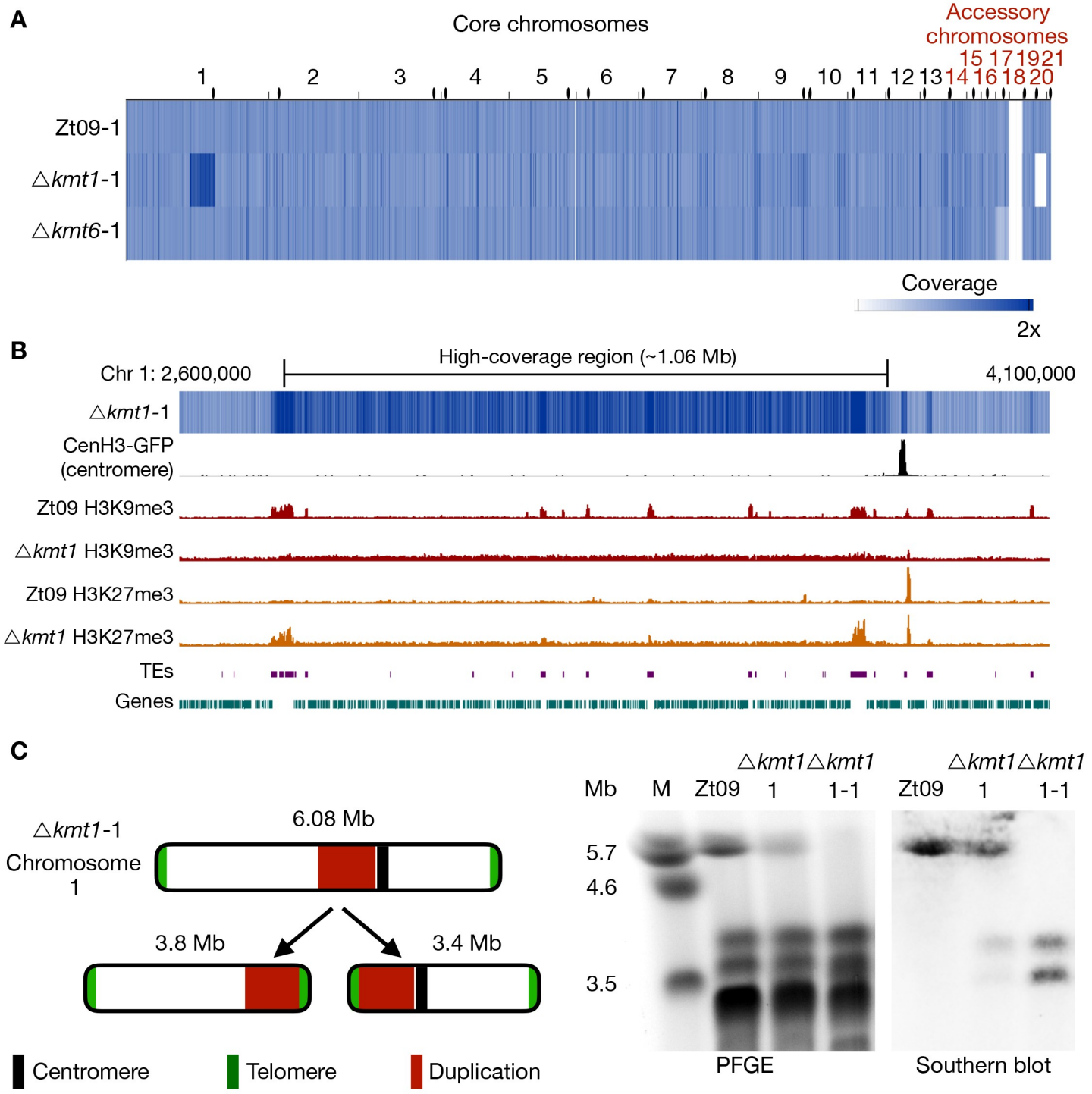

Fig 4. Genome sequencing of progenitor strains for the long-term growth experiment and analysis of structural variation in the *Δkmt1* progenitor. (A) The genomes of progenitor strains were sequenced and reads were mapped to the reference genome. Genome coverage was normalized to 1x coverage to allow identification and comparison of differences within and between strains. All strains were missing chromosome 18, as expected [41]. Δ*kmt6* had lower coverage (0.4x) of chromosome 17. *Δkmt1* lost chromosome 20 and, most notably, showed a long segment (~ 1Mb) of high-coverage (1.6x) on chromosome 1. Centromeres are indicated as black dots. **(B)** Examination of the high-coverage region breakpoints on chromosome 1. The first breakpoint located within a TE-rich region that is enriched with H3K9me3 in Zt09 and showed new enrichment with H3K27me3 in *Δkmt1*. The second breakpoint is within a gene-rich region in close proximity to relocalized H3K27me3 and very close to the centromere (~15 kb). **(C)** Further analysis of this high-coverage region revealed *de novo* telomere formation at the breakpoints indicating a chromosome breakage at both ends of the high-coverage region. To validate chromosome breakage and possible new chromosome formation, we conducted PFGE and separated the large chromosomes

of Zt09, of the *Δkmt1* progenitor strain (*Δkmt1*-1) and of a single clone originating from the *Δkmt1* progenitor strain stock (*Δkmt1*-1-1). Chromosome 1 (~6 Mb) is present in Zt09 and *Δkmt1*-1 (faint band), but not in the *Δkmt1*-1-1 single clone. We conducted Southern analysis on the PFGE blot using a sequence of the high-coverage region as a probe. It hybridized to the original chromosome 1 band in Zt09 and *Δkmt1*-1, but additionally to a ~3.4 Mb and ~3.8 Mb band in *Δkmt1*-1 and only to these bands in *Δkmt1*-1-1. This confirmed the formation of new chromosomes, both containing the high-coverage region in some cells of the progenitor strain population.

https://doi.org/10.1371/journal.pgen.1008093.g004

sequenced pool of cells, suggesting loss of chromosome 17 in ~40% of the sequenced Δ*kmt6* cells, a chromosome loss that likely occurred at the very beginning of the experiment.

Unexpectedly, the Δ*kmt1* progenitor displayed a long high-coverage (~1.6x) region on chromosome 1 (Fig 4), suggesting that the region had been duplicated in ~60% of the sequenced Δ*kmt1* cells. Furthermore, this genome has a shorter chromosome 6 and does not contain chromosome 20 (Fig 4A, S9 Table). The presence of this kind of structural variation in the progenitor strain is indicative for a high degree of genome instability in absence of Kmt1. Analysis of discordant reads mapped to both ends of the ~1 Mb high-coverage region on chromosome 1 revealed telomeric repeats ($TTAGGG_n$), suggesting the formation of *de novo* telomeres. Pulsed-field gel electrophoresis (PFGE) and Southern analyses confirmed the formation of two new independent chromosomes both containing the high-coverage region and either the right or left arm of chromosome 1 (Fig 4C). The breakpoint on the left side coincides with a large TE-rich region that is associated with H3K9me3 in the wild type. Both breakpoints coincide with or are in close proximity to regions that show enrichment of relocated H3K27me3 in the *Δkmt1* mutant (Fig 4B), suggesting a possible link between relocated H3K27me3 and genome instability.

After six months of vegetative growth, we sequenced the pooled genomes of all nine 'evolved' populations. We found no evidence for large-scale genomic rearrangements in any of the evolved Zt09 or Δ*kmt6* populations (Fig 5A). Apart from seven small deletions or duplications (S9 Table), the largest structural variation found in one of the evolved Δ*kmt6* populations (Δ*kmt6* 50–2), was a partial loss (~18 kb) at the right end of chromosome 15. However, we found variation in the read coverage of accessory chromosomes in all sequenced genomes indicating whole chromosome losses in individual cells of the sequenced population. The distinct dynamics of individual accessory chromosome losses were described in the previous section as part of the short-term growth results (Table 2).

In contrast to the few variations detected in the Zt09 and Δ*kmt6* populations, we found numerous large-scale high-coverage regions on different core chromosomes, chromosome breakages followed by *de novo* telomere formation, chromosomal fusions, as well as several smaller deletions and duplications in the evolved Δ*kmt1* populations (Fig 5A, S9 Table). All three evolved Δ*kmt1* populations have large duplicated regions on chromosome 1 (Fig 6), but their locations as well as the resulting structural variations differ from the one identified in the progenitor strain (Fig 6A). This can be explained by independent events, as not all Δ*kmt1* progenitor cells underwent the rearrangement of chromosome 1 (Fig 4C), or by continuous structural rearrangement events as a consequence of the presence of large duplicated regions in the genome. Analyses of the affected regions and breakpoints indicate a connection between the structural variations of progenitor (compared to the reference) and evolved strains. In all evolved Δ*kmt1* populations, duplicated regions fully or partially overlap with the high-coverage region of the progenitor strain (Fig 6A–6D).

Since populations reflect a mixture of distinct genotypes, we also sequenced three single Δ*kmt1* clones originating from the populations from transfer 50 to characterize the structural variation in more detail (Fig 5B). The single clones were selected based on different PFGE karyotypes (S9 Fig) and originated from population *Δkmt1*-50-1 (Δ*kmt1*-50-1-1) and Δ*kmt1*-50-2 (Δ*kmt1*-50-2-1 and Δ*kmt1*-50-2-2). As two of these single clones (Δ*kmt1*-50-1-1 and Δ*kmt1*-

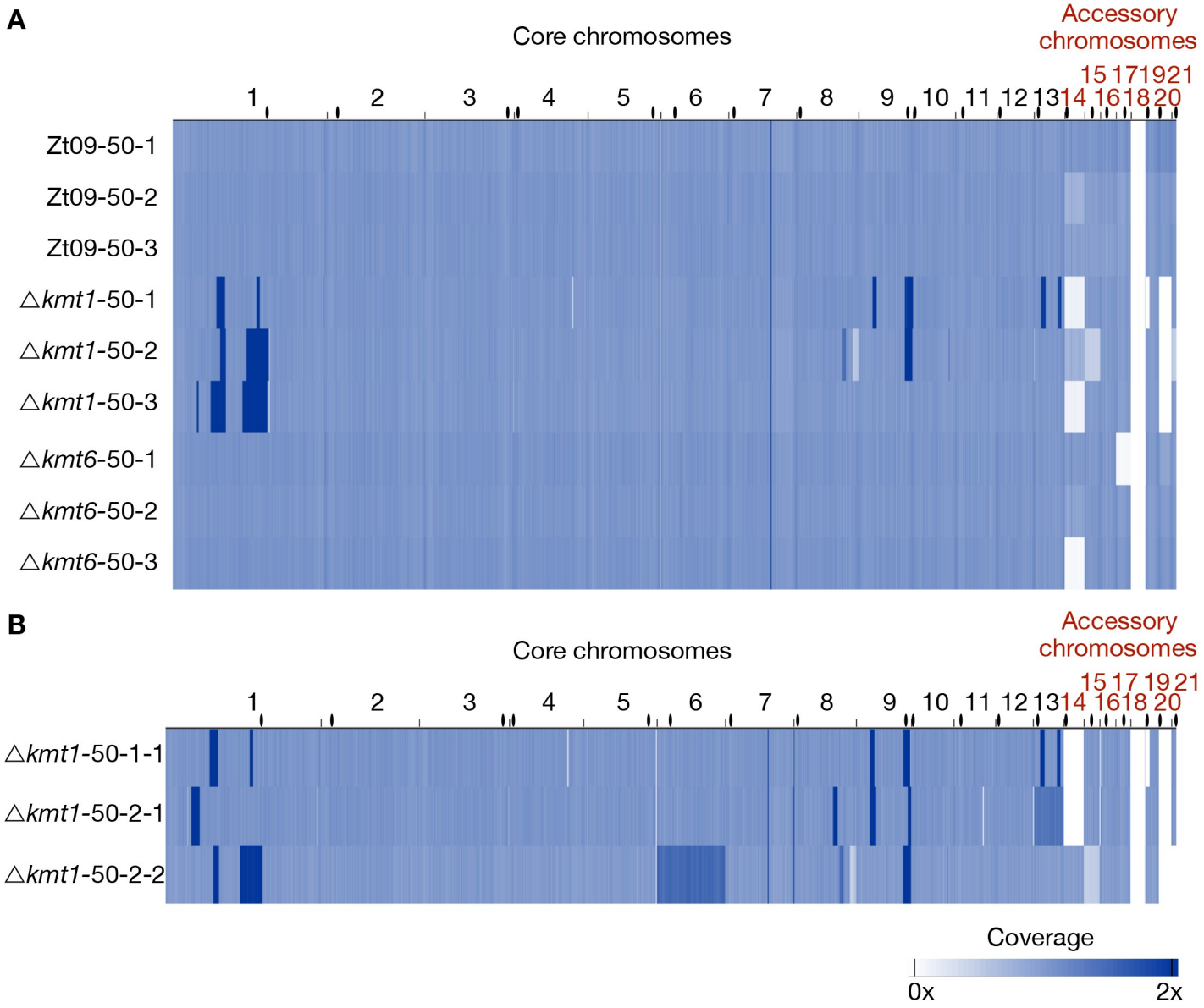

Fig 5. Genome sequencing of evolved populations and single clones originating from the long-term growth experiment. (A) Genomes of each replicate population after 50 transfers were sequenced and mapped to the reference. Coverage is normalized to 1x. Except for coverage differences on the accessory chromosomes, there were no large structural variations detectable for the evolved Zt09 and *Δkmt6* populations. In contrast, *Δkmt1* populations contained multiple high-coverage regions (dark blue) on core chromosomes as well as large deletions indicated by low (light blue) or no (white) coverage. **(B)** To further characterize structural variation in the evolved *Δkmt1* strains, three single clones originating from populations *Δkmt1*-50-1 (*Δkmt1*-50-1-1) and *Δkmt1*-50-2 (*Δkmt1*-50-2-1 and *Δkmt1*-50-2-2) were sequenced. Clones *Δkmt1*-50-1-1 and *Δkmt1*-50-2-2 show a very similar pattern as their respective populations, while *Δkmt1*-50-2-1 resembles a genotype that appears to be rare in population *Δkmt1*-50-2. High coverage on entire core chromosomes 13 (*Δkmt1*-50-2-1, 1.3x coverage) and 6 (*Δkmt1*-50-2-2, 1.5x coverage) indicates whole core chromosome duplications that were maintained in some nuclei. Centromeres are indicated as black dots.

https://doi.org/10.1371/journal.pgen.1008093.g005

50-2-2) largely resemble the genotypes found in their respective populations, we conclude the presence of a predominant genotype in each evolved replicate population. However, Δ*kmt1*-50-2-1 clearly differs from this genotype and therefore reveals the existence of additional, rarer genotypes in the evolved populations. Relatively small deletions and duplications (up to 30 kb) as well as chromosome breakage followed by *de novo* telomere formation were found on

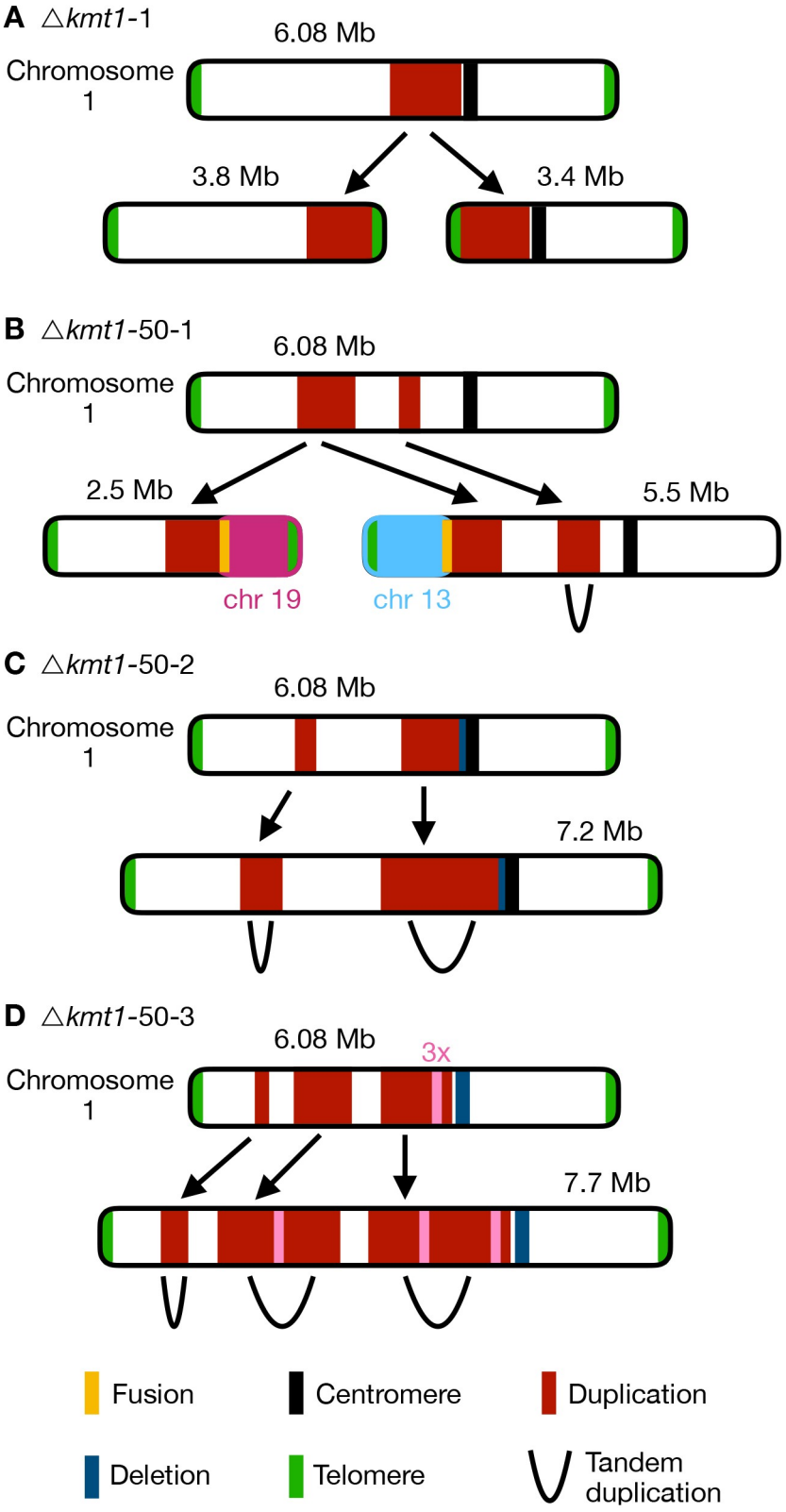

Fig 6. Different outcomes of structural variation of chromosome 1 in evolved *Δkmt1* strains. Upper chromosome maps display coverage differences based on mapping to the reference genome including duplication indicated by

higher read coverage (red) and deletion indicated by lower coverage (blue). The respective lower maps show structural rearrangements predicted by our structural variant analysis. **(A)** In the progenitor strain, a duplicated region was involved in the formation of two new chromosomes. At both termini of the duplication the chromosome broke and telomeric repeats were added *de novo* to these breakpoints (see Fig 4). Thus, two new chromosomes were formed, both containing the duplicated sequence. This structural variation was not found in all cells in the Δ*kmt1* progenitor strain and the structural variation that arose in the evolved strains **(B-D)** can therefore be the result of rearrangements of the reference chromosome 1 or the two newly formed chromosomes. **(B)** In the evolved population Δ*kmt1*-50-1, two duplicated sequences were detected. The borders of the first region mark chromosome breakages that were fused to telomeres of other chromosomes. The first breakpoint was attached to the telomere of chromosome 13 forming a new 5.5 Mb chromosome while the second breakpoint was fused to the telomere of chromosome 19 (new 2.5 Mb chromosome). The second duplicated region represented a tandem duplication located on the new 5.5 Mb chromosome that falls within the duplicated region of the progenitor strain. **(C)** Population Δ*kmt1*-50-2 contained two duplicated regions, that both resembled tandem duplications. The second duplication is very similar to the one found in the progenitor strain but includes half of the centromere and had a deletion, where the breakpoint close to the centromere in the progenitor strain is located. **(D)** Population Δ*kmt1*-50-3 displayed three duplicated sequences that all form tandem duplications resulting in the formation of a 7.7 Mb version of chromosome 1. The third duplicated region was, as in population Δ*kmt1*-50-2, very similar to the one in the progenitor strain. However, in this case the complete centromere-associated sequence was deleted. Furthermore, a ~50 kb region inside the third duplicated region exhibited 3x sequencing coverage and was found in between the tandem duplication of the second duplicated region (see S9 Table).

https://doi.org/10.1371/journal.pgen.1008093.g006

almost all chromosomes. These occurred mainly linked to annotated TEs (S10 Table) whereby loss of H3K9me3 likely promoted instability. However, major rearrangements, including chromosomal fusions, were always linked to large segmental duplications (S10 Fig). In two strains we detected higher coverage of entire core chromosomes indicating core chromosome duplications (Fig 5B). Results from read coverage (S10 Table) and PCR analyses indicate that Δ*kmt1*-50-2-2, as well as the majority of the Δ*kmt1*-50-2 population, may have undergone a whole genome duplication.

To investigate whether the underlying sequence is involved in the formation of large-scale rearrangements, we analyzed the breakpoints of each duplicated region. The location of breakpoints does not show a clear TE-associated pattern as observed for the smaller deletions or chromosome breakages. Out of 28 analyzed breakpoints, only seven are directly located within annotated TEs, while thirteen fall into genes, seven are intergenic and one is located in the centromere (S11 Table). Considering all structural rearrangements in the three sequenced single clones, we found that out of 62 events, 34 were associated (direct overlap or <5 kb distance) to regions that show enrichment for H3K27me3 (S12 Table). Based on these observations, we hypothesize that two non-exclusive pathways, namely TE-associated instability caused by loss of H3K9me3 or invasion of H3K27me3, may serve as initial events, which are followed by continuous rearrangements possibly caused by increased mitotic recombination activity and deficiency in DNA repair resulting in a spectrum of structural variation (S11 Fig).

Discussion

H3K27me3 destabilizes accessory chromosomes

We investigated the effects of loss of two important heterochromatin-associated histone modifications, H3K9me3 and H3K27me3, on chromatin organization, transcription and genome stability and characterized phenotypes of the deletion mutants. Loss of H3K9me3 allows relocalization of H3K27me3 in *kmt1* deletion mutants, which has great impact on genome and chromosome stability, resulting in numerous large-scale rearrangements. In contrast, the genomes of evolved Δ*kmt6* and Zt09 strains revealed only few and relatively minor changes. Unexpectedly, the presence of H3K27me3 impacts chromosome stability by either destabilizing whole chromosomes in normal cells, supported by the high loss-rate in the reference strain compared to the Δ*kmt6* mutants, or by mislocalization as shown by the increased sequence

instability in the Δ*kmt1* mutants. Taken together, enrichment with H3K27me3 in wild type cells is a main driver of mitotic chromosome instability.

We propose different scenarios for how chromosomes may get lost during mitosis and how H3K27me3 may be linked to these processes. For example, accessory chromosomes may not be accurately replicated whereby only one sister chromatid is transmitted. Alternatively, non-disjunction of sister chromatids during mitosis produces one cell with two copies and one cell lacking the respective chromosome. Previous cytology on *Z. tritici* strains expressing GFP-tagged CENPA/CenH3 protein suggested that core and accessory chromosomes may be physically separated in the nucleus [31]. Previous studies showed that H3K27me3-enriched chromatin localizes near the nuclear periphery, and loss of H3K27me3 enables movement of this chromatin to the nucleus core in mammals and fungi [52,53]. Proximity to the nuclear membrane and heterochromatic structure can furthermore result in differential, and often late, replication timing [54,55]. Loss of H3K27me3 and the correlated movement to the inner nuclear matrix may alter replication dynamics of accessory chromosomes resulting in higher rates of faithfully replicated chromosomes and lower rates of mitotic loss (Fig 7).

Heterochromatic regions, especially associated with H3K27me3, tend to cluster together and form distinct foci in the nucleus of *Drosophila melanogaster* visualized by cytology [56,57], and loss of H3K27me3 reduces interaction between these regions [58]. We hypothesize that enrichment of H3K27me3 on the entire accessory chromosomes maintains physical interactions that persist throughout mitosis. This may decrease the efficiency of separation of sister chromatids resulting in loss of the chromosome in one cell and a duplication in the other cell. So far, we have focused our screening on chromosome losses but determining the exact rates of accessory chromosome duplications is necessary to test this hypothesis. Genome sequencing of *Z. tritici* chromosome loss strains revealed that duplications of accessory chromosomes can occur [46]. Similarly, B chromosomes in rye are preferentially inherited during meiosis by non-disjunction of sister chromatids during the first pollen mitosis [59], indicating that deviation from normal chromosome segregation occurs. Accessory chromosomes are commonly found in natural isolates of *Z. tritici*, despite the high loss rates we demonstrated during mitotic growth [46]. This observation implies the presence of other mechanisms that counteract the frequent losses of accessory chromosomes. Recent analyses of meiotic transmission showed that unpaired accessory chromosomes are transmitted at higher rates in a uniparental way [60,61]. We propose that H3K27me3 is involved in accessory chromosome instability and transmission both during mitosis and meiosis by influencing nuclear localization of chromosomes and thereby altering replication or transmission (Fig 7). Future analyses with fluorescently tagged core and accessory chromosomes and by chromosome conformation capture (Hi-C) will shed light on nuclear interactions and chromosome transmission dynamics. As not all accessory chromosomes, despite being enriched with H3K27me3, are lost at the same rate, we note that additional mechanisms likely contribute to accessory chromosome dynamics.

H3K9me3 loss allows invasion by H3K27me3 and results in genome instability

While loss of H3K27me3 resulted in only minor differences to wild type growth and, unexpectedly, rather promoted than decreased genome stability, we detected a high number of smaller (up to 30 kb) deletions and duplications, chromosome breakages and several gross chromosomal rearrangements linked to large duplications in the Δ*kmt1* mutants. Absence of H3K9me2/3 has been associated with chromosome and genome instability in other organisms [13,14,62,63]. Smaller deletions, duplications and chromosome breakages resulting in

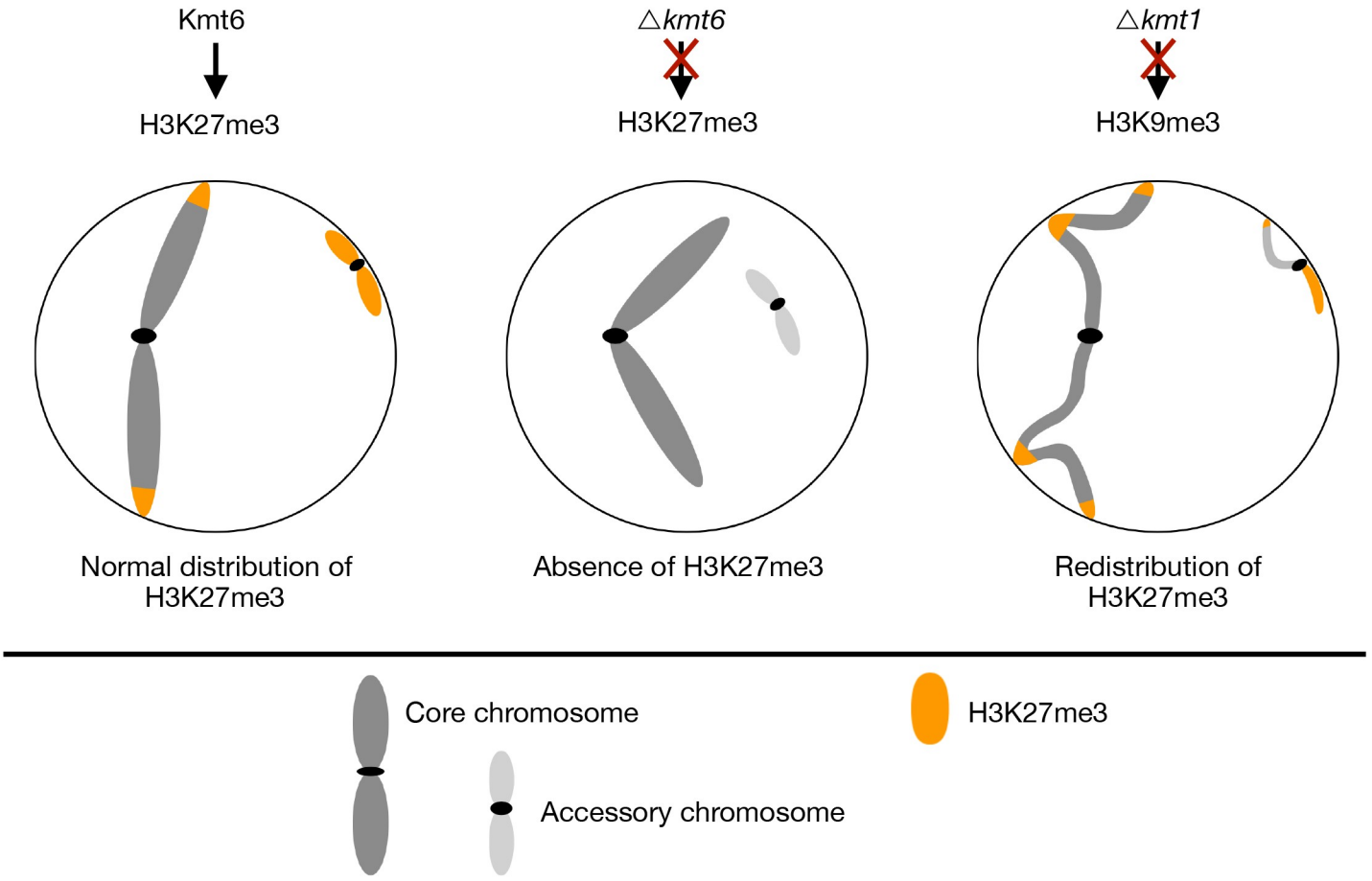

Fig 7. Working model to illustrate how H3K27me3 may influence nuclear localization of whole chromosomes or landmark genomic regions. In wildtype cells (left panel), H3K27me3 is localized in subtelomeric regions and on accessory chromosomes, directing those regions to the nuclear periphery and resulting in increased instability of these regions. Loss of H3K27me3 (middle panel) results in a relocation of former H3K27me3-enriched sequences to the inner nucleus and an increase of genome stability. Loss of the histone modification H3K9me3 enables H3K27me3 to spread, leading to mislocalization of H3K27me3, altered physical localization and chromatin interactions in the nucleus that fuel genome instability of these regions (right panel).

https://doi.org/10.1371/journal.pgen.1008093.g007

shortened chromosomes due to loss of chromosome ends that we identified in the Δ*kmt1* mutants, correlate with TEs, enriched with H3K9me3 in wild type. Replication of heterochromatin-associated DNA is challenging for the cell as repetitive sequences may form secondary structures that can stall the replication machinery [64]. Consequently, instability of repeated sequences has been linked to errors during DNA replication [65–67]. Furthermore, the structural variation that arises depends on the mode of DNA repair following the DNA damage [68,69]. The structural rearrangements detected in the Δ*kmt1* mutants indicate that repair of double-strand breaks involves both non-homologous end joining and *de novo* telomere formation. We propose that the main factor for genome instability is replication-associated instability of repeated sequences subsequently promoting the formation of large-scale rearrangements (S11 Fig).

Not all breakpoints of rearrangements, especially of the large duplicated sequences, were associated with TEs, however. We found that duplicated sequences in the experimentally evolved Δ*kmt1* mutants fully or partially overlap with the duplicated regions of the Δ*kmt1* progenitor strain. This suggests that structural variations are subject to continuous

rearrangements, resulting in rearrangements no longer directly linked to the initial event. We note that the rearrangements and genotypes we detected are the result of selection during our long-term growth experiments and thus do not necessarily reflect the full spectrum of rearrangements occurring in *Δkmt1* mutants; many additional structural variants may have disappeared quickly from the population or included lethal events.

Concomitant with loss of H3K9me3 in the Δ*kmt1* strains, we found relocalization of H3K27me3 to former H3K9me3 regions. A similar redistribution of H3K27me3 in absence of heterochromatin factors has been reported in plants and animals [70–72] and other fungi [22,27,73]. In *N. crassa*, redistribution of H3K27me3 in a Δ*kmt1* (*dim-5*) mutant background results in severe growth defects and increased sensitivity to genotoxic stress that can be rescued by elimination of H3K27me3, indicating that aberrant H3K27me3 distribution severely impacts cell viability [27]. Although we did not see rescue of phenotypic defects observed *in planta* or in *in vitro* stress assays in the Δ*k1/k6* double mutants, the chromosome-loss rate was reduced compared to *Δkmt1* mutants, suggesting a stabilizing effect when H3K27me3 is absent. We found that some breakpoints of the rearrangements in the Δ*kmt1* mutants without H3K9me3 also show enrichment with the invading H3K27me3. This finding also suggests that sequences associated with H3K27me3 are more susceptible to genome instability. Regions enriched with H3K27me3 have been shown to exhibit a high degree of genetic variability in form of mutations, increased recombination, or structural variation compared to the rest of the genome [21,23,30,31,74–76]. Experimental evolution in *Fusarium fujikuroi* showed that increased H3K27me3 levels in subtelomeric regions coincided with increased instability [77] and we previously detected a highly increased rate of chromosomal breakage under stress conditions in subtelomeric H3K27me3 regions in *Z. tritici* [46]. These observations together with our findings strongly indicate that H3K27me3 plays a pivotal role in decreasing genome stability.

In summary, the presence of Kmt1 and H3K9me3 respectively, is essential to maintain genome integrity in this fungus. TE-mediated rearrangements may be involved in the genetic variability detected in *Z. tritici* isolates [78–80] and have been suggested as drivers of genome evolution in various species [81–83]. Our findings concerning the role of H3K9me3 for genome stability provide a basis for future studies focusing on the influence of heterochromatin on structural genome rearrangements using *Z. tritici* as a model organism. We found that, unlike for H3K9me3, presence and not absence of H3K27me3 is linked to genome instability. Surprisingly, loss of H3K27me3 does not result in dramatic changes of overt phenotypes and is also not clearly linked to transcriptional activation in *Z. tritici*. This allowed us to uncouple the transcriptional and regulatory effects of H3K27me3 from the influence on chromatin stability and will in the future result in further mechanistic insights on the influence of histone modifications on chromosome stability.

Materials and methods

Culturing conditions of fungal and bacterial strains

Zymoseptoria tritici strains were cultivated on solid (2% [w/v] Bacto agar) or in liquid YMS medium (0.4% [w/v] yeast extract, 0.4% [w/v] malt extract, 0.4% [w/v] sucrose). Liquid cultures were inoculated from plate or directly from glycerol stocks and grown for 3–4 days at 18˚C in a shaking incubator at 200 rpm. Plates were inoculated from glycerol stocks and grown for 5–6 days at 18˚C. *Escherichia coli* TOP10 cells were grown overnight in dYT (1.6% [w/v] tryptone, 1% [w/v] yeast extract, 0.5% [w/v] NaCl and 2% Bacto agar for solid medium) supplemented with antibiotics for plasmid selection (40 μg/mL kanamycin) at 37˚C and at 200 rpm for liquid cultures. *Agrobacterium tumefaciens* strain AGL1 was grown in dYT containing

rifampicin (50 μg/mL) and carbenicillin (100 μg/mL) supplemented with antibiotics for plasmid selection (40 μg/mL kanamycin) at 28˚C at 200 rpm in liquid culture for 18 h and on plate at 28˚C for two days.

Transformation of *Z. tritici*

Z. tritici deletion and complementation strains were engineered using *A. tumefaciens*-mediated transformations as described before [49,84]. Flanking regions of the respective genes were used to facilitate homologous recombination for integration at the correct genomic location. The plasmid pES61 (a derivate of the binary vector pNOV-ABCD [49]) was used for targeted gene deletion and complementation. Plasmids were assembled using a restriction enzyme-based approach or Gibson assembly [85]. Plasmids were amplified in *E. coli* TOP10 cells and transformed in the *A. tumefaciens* strain AGL1 as described previously [86]. Gene deletions of *kmt1* (*Zt09_chr_1_01919*) and *kmt6* (*Zt09_chr_4_00551*) were facilitated by replacement of the respective ORF with a hygromycin resistance cassette (*hph*). The *kmt1/kmt6* double deletion mutant was constructed by integrating a nourseothricin resistance cassette (*nat*) replacing *kmt1* in a *kmt6* deletion mutant background. Complementation constructs containing the respective gene and a G418 resistance cassette (*neo*) were integrated at the native loci in the deletion strains. All plasmids and strains constructed in this study are listed in S1 Table. Transformed strains were screened by PCR for correct integrations of the construct followed by Southern blot [87] with probes generated by DIG labeling (Roche, Mannheim, Germany) following manufacturer's instructions.

DNA isolation for PCR screening and southern blotting

For rapid PCR screening (candidates for transformation and chromosome loss), a single *Z. tritici* colony was resuspended in 50 μL of 25 mM NaOH, incubated at 98˚C for 10 min and afterwards 50 μL of 40 mM Tris-HCl pH 5.5 were added. Four μl of the mix was used as template for PCRs. For DNA extraction for Southern blotting, we used a standard phenol-chloroform extraction protocol [88] for DNA isolation.

Phenotypic characterization *in vitro*

For the *in vitro* growth assays, liquid YMS cultures were inoculated with 100 cells/μL (OD_{600} = 0.01); cells were grown in 25 mL YMS at 18˚C and 200 rpm. For each mutant and complementation strain, two transformants (biological replicates), and three replicate cultures per transformant (technical replicates) were used. For the reference strain Zt09, two separate pre-cultures were grown as biological replicates and each pre-culture was used to inoculate three replicate cultures. OD_{600} was measured at different time points throughout the experiment until the stationary phase was reached. The R package growthcurver [89] was used to fit the growth curve data enabling to compare *in vitro* growth of the different strains.

To test the tolerance of mutant and reference strains towards different stressors, we performed an *in vitro* stress assay on YMS plates. Each plate contained additives constituting different stress conditions. Cell suspensions containing $10^7/10^8$ cells/mL and a tenfold dilution series down to 100 cells/mL were prepared; 3 μL of each dilution were pipetted on solid YMS containing the following additives: 0.5 M NaCl, 1 M NaCl, 1 M sorbitol, 1.5 M sorbitol, 1.5 mM H_2O_2, 2 mM H_2O_2, 300 μg/mL Congo red, 0.01% MMS (methyl methane sulfonate), 0.025% MMS, 1 μg/mL actinomycin D and 1.5 μg/mL actinomycin D. Furthermore, we included a H_2O-agar (2% bacto agar) plate. All plates were incubated at 18˚C for six days, except for one YMS plate that was incubated at 28˚C to test for thermal stress responses.

Phenotypic characterization *in planta*

Seedlings of the susceptible wheat cultivar Obelisk (Wiersum Plantbreeding BV, Winschoten, The Netherlands) were potted (three plants per pot) after four days of pre-germination and grown for seven more days. Single cell suspensions of mutant and reference strain were prepared (10^8 cells / mL in H_2O with 0.1% Tween 20) and brush inoculated on a marked area of the second leaf. Following inoculation, the plants were incubated in sealed plastic bags containing ~ 1 L of H_2O for 48 h providing high humidity to promote infections. Growth conditions for the plants throughout the complete growth phase and infection were 16 h light (200 μmol/$m^{-2}s^{-1}$) and 8 h dark at 20˚C and 90% humidity. First appearances of symptoms, necrosis or pycnidia, were assessed by manual inspection of every treated leaf. 21 or 28 days post infection, inoculated leaves were finally screened for infection symptoms. Visual inspection of each leaf was performed to evaluate the percentage of leaf area covered by necrosis and pycnidia. Six different categories were differentiated based on the observed coverage (0: 0%, 1: 1–20%, 2: 21–40%, 3: 41–60%, 4: 61–80%, 5: 81–100%). Furthermore, automated symptom evaluation was performed by analysis of scanned images of infected leaf areas as described previously [90].

Long-term evolution experiment

For the long-term evolution experiment (~6 months), cells were inoculated directly from the glycerol stocks into 20 mL liquid YMS cultures. We used Zt09, Δ*kmt6* (#285) and Δ*kmt1* (#68), each strain grown in triplicates. Every three to four days, cells were transferred to new YMS medium. Cells were grown at 18˚C and 200 rpm. For every transfer, cell density of the cultures was measured by OD_{600} and the new cultures were inoculated with a cell density of ~ 100 cells / μL (correlating to a transfer of 0.1% of the population). After 50 transfers, the genomes of the evolved populations and each progenitor strain were sequenced. Additionally, three genomes of single clones derived from the *Δkmt1* populations after 50 transfers were sequenced to characterize genome rearrangements in more detail.

Short-term evolution experiment

For the short-term evolution experiment over a time period of four weeks, cultures were inoculated from single colonies grown on solid YMS. Zt09, *Δkmt6* (#285), *Δkmt1* (#80), *Δk1*/Δk6 (#23) double mutant, *kmt1*$^+$ (#42) and *kmt6*$^+$ (#11) were grown in triplicate YMS cultures. For this experiment we used a different independent *Δkmt1* mutant clone (#80), as we discovered that the strain used in the previous long-term evolution experiment (#68) was missing chromosome 20. Every three to four days, 900 μL culture were transferred to 25 mL fresh YMS (correlating to a transfer of ~ 4% of the population). After four weeks of growth (including eight transfers to new medium) at 18˚C and 200 rpm, cultures were diluted and plated on YMS agar to obtain single colonies. These single colonies were PCR screened for presence of accessory chromosomes as described in [46].

Pulsed-field gel electrophoresis (PFGE)

Cells were grown in YMS medium for five days and harvested by centrifugation for 10 min at 3,500 rpm. We used 5 x 10^8 cells for plug preparation that were washed twice with Tris-HCl, pH 7.5, resuspended in 1 mL TE buffer (pH 8) and mixed with 1 mL of 2.2% low range ultra agarose (Bio-Rad, Munich, Germany). The mixture was pipetted into plug casting molds and cooled for 1 h at 4˚C. Plugs were placed to 50 mL screw cap Falcon tubes containing 5 mL of lysis buffer (1% SDS; 0.45 M EDTA; 1.5 mg/mL proteinase K [Roth, Karlsruhe, Germany])

and incubated for 48 h at 55˚C while the buffer was replaced once after 24 h. Chromosomal plugs were washed three times for 20 min with 1 X TE buffer before storage in 0.5 M EDTA at 4˚C. PFGE was performed with a CHEF-DR III pulsed-field electrophoresis system (BioRad, Munich, Germany). Separation of mid-size chromosomes was conducted with the settings: switching time 250 s– 1000 s, 3 V/cm, 106˚ angle, 1% pulsed-field agarose in 0.5 X TBE for 72 h. Large chromosomes were separated with the following settings: switching time 1000 s– 2000 s, 2 V/cm, 106˚ angle, 0.8% pulsed-field agarose in 1 X TAE for 96 h. *Saccharomyces cerevisiae* chromosomal DNA (BioRad, Munich, Germany) was used as size marker for the for mid-size chromosomes, *Schizosaccharomyces pombe* chromosomal DNA (BioRad, Munich, Germany) for the large chromosomes. Gels were stained in ethidium bromide staining solution (1 μg/mL ethidium bromide in H_2O) for 30 min. Detection of chromosomal bands was performed with the GelDocTM XR+ system (Bio-Rad, Munich, Germany). Southern blotting was performed as described previously [87] but using DIG-labeled probes generated with the PCR DIG labeling Mix (Roche, Mannheim, Germany) following the manufacturer's instructions.

ChIP-sequencing

Cells were grown in liquid YMS medium at 18˚C for 2 days until an OD_{600} of ~ 1 was reached. Chromatin immunoprecipitation was performed as previously described [91] with minor modifications. We used antibodies against H3K4me2 (#07–030, Merck Millipore), H3K9me3 (#39161, Active Motif) and H3K27me3 (#39155, Active Motif). ChIP DNA was purified using SureBeads Protein G Magnetic Beads (Bio-Rad, Munich, Germany) and, replacing phenol/chloroform extractions, we used the ChIP DNA Clean & Concentrator Kit (Zymo Research, Freiburg, Germany). We sequenced two biological and one additional technical replicate for Zt09, Δ*kmt1*, Δ*kmt6*, and the Δ*k1*/*k6* strains. Sequencing was performed at the OSU Center for Genome Research and Biocomputing on an Illumina HiSeq2000 or HiSeq3000 to obtain 50-nt reads and at the Max Planck Genome Center, Cologne, Germany (https://mpgc.mpipz.mpg.de/home/) on an Illumina Hiseq3000 platform obtaining 150-nt reads (S2 Table).

RNA-sequencing

For RNA extraction, cells were grown in liquid YMS at 18˚C and 200 rpm for two days until an OD_{600} of ~ 1 was reached. Cells were harvested by centrifugation and ground in liquid nitrogen. Total RNA was extracted using TRIzol (Invitrogen, Karlsruhe, Germany) according to manufacturer's instructions. The extracted RNA was further DNAse-treated and cleaned up using the RNA Clean & Concentrator-25 Kit (Zymo Research, Freiburg, Germany). RNA samples of two biological replicates of Zt09, Δ*kmt1*, Δ*kmt6*, and the Δ*k1*/*k6* double mutant were sequenced. Poly(A)-captured, stranded library preparation and sequencing were performed by the Max Planck-Genome-centre Cologne, Germany (https://mpgc.mpipz.mpg.de/home/) on an Illumina Hiseq3000 platform obtaining ~ 20 million 150-nt reads per sample (S2 Table).

Genome sequencing

Genomic DNA for sequencing was prepared as described previously [92]. Library preparation and genome sequencing of the progenitor strains used for the evolution experiments were performed at Aros, Skejby, Denmark using an Illumina HiSeq2500 platform obtaining 100-nt paired-end reads. Library preparation (PCR-free) and sequencing of the evolved populations and the three evolved single *Δkmt1* mutants were performed by the Max Planck Genome Center, Cologne, Germany (https://mpgc.mpipz.mpg.de/home/) on an Illumina HiSeq3000 platform resulting in 150-nt paired-end reads (S2 Table).

Short read mapping and data analysis

A detailed list of all programs and commands used for mapping and sequencing data analyses can be found in the supplementary text S1. All sequencing data was quality filtered using the FastX toolkit ((http://hannonlab.cshl.edu/fastx_toolkit/) and Trimmomatic [93]. RNA-seq reads were mapped using hisat2 [94], mapping of ChIP and genome data was performed with Bowtie2 [95]. Conversion of sam to bam format, sorting and indexing of read alignments was done with samtools [96].

To detect enriched regions in the ChIP mappings, we used HOMER [97]. Peaks were called individually for replicates and merged with bedtools [98]. Only enriched regions found in all replicates were considered for further analyses. Genome coverage of enriched regions and overlap to genes and TEs was calculated using bedtools [98].

We used cuffdiff [99] to calculate RPKM values and to estimate expression in the different strains. Raw reads mapping on genes and TEs were counted by HTSeq [100], differential expression analysis was performed in R [101] with DESeq2 [102]. Cutoff for significantly differentially expressed genes was padj < 0.001 and $|\log2 \text{ fold-change}| > 2$. The R package topGO [103] was used to perform gene ontology enrichment analyses. Fisher's exact test (p-value < 0.01) was applied to detect significantly enriched terms in the category 'biological process'.

To detect structural variation in the sequenced genomes, we used SpeedSeq [104] and LUMPY [105]. All detected variation was further verified by manual visual inspection. Visualization was performed with the integrative genome browser (IGV) [106].

Supporting information

S1 Table. Plasmids, strains and primer designed for this study. Listed are all primers used to create plasmids and probes for Southern blots.
(XLSX)

S2 Table. Statistics and overview of sequencing data generated in this study.
(XLSX)

S3 Table. RPKM values of all genes of Zt09 reference and mutant strains. RPKM was calculated using cuffdiff (see Material and Methods).
(XLSX)

S4 Table. Genes associated to either H3K9me3 or H3K27me3 in Zt09 or mutant strains.
(XLSX)

S5 Table. Deseq2 results to identify differentially expressed genes between Zt09 reference and mutant strains. Comparisons were performed pair-wise, genes were considered to be significantly different expressed, when log2 fold-change > 2 and padj < 0.001.
(XLSX)

S6 Table. Enriched GO terms and upregulated genes in the categories DNA integration and RNA-dependent DNA replication.
(XLSX)

S7 Table. Deseq2 results to analyze expression of TEs in Zt09 reference and mutant strains. Comparisons were performed pair-wise.
(XLSX)

S8 Table. Predicted secondary metabolite gene clusters merged with the *Z. tritici* annotation.
(XLSX)

S9 Table. Structural variation detected in sequenced progenitor and evolved strains. Listed are location, size and type of structural variation. Only events that have not been described before for Zt09 are listed here.
(XLSX)

S10 Table. Detailed description and annotation of structural variation detected in the single *kmt1* deletion clones. Some structural variations are associated to large segmental duplications. This is noted as (large segmental duplication).
(XLSX)

S11 Table. Annotation of breakpoints of segmental duplications in the single clones originating from evolved populations △*kmt1*-50-1 and △*kmt1*-50-2.
(XLSX)

S12 Table. Distance of structural rearrangements in the evolved single △kmt1 clones to H3K9me3 (Zt09) and H3K27me3 (Zt09 and △*kmt1*).
(XLSX)

S1 Supplementary Text. Data analysis–programs and commands used for analysis of ChIP-seq, RNA-seq and genome sequencing data.
(PDF)

S1 Fig. Overview of experiments, key findings and corresponding figures and tables in this study.
(PDF)

S2 Fig. Southern blots to confirm correct integration of deletion and complementation constructs: for deletion of *kmt1* **(A)**, complementation of *kmt1* **(B)**, deletion of *kmt1* in a *kmt6* deletion background resulting in the generation of a double deletion mutant **(C),** deletion of *kmt6* **(D)**, and complementation of *kmt6* **(E).** The left blot verifying the deletion of *kmt6* (D) displays two bands instead of one for the wildtype Zt09. This is likely due to incomplete digestion, as a second blot (on the right) using the same enzymes and probes only results in the correct band for Zt09. Depictured are genomic locations of wildtype (Zt09) and mutant strains, restriction enzymes used, probes, and expected fragment sizes on the blots. All tested strains, except for the underlined, were verified as correct mutants. The strains used for experiments in this study are highlighted in **bold**.
(PDF)

S3 Fig. Verification of absence of H3K9me3 and H3K27me3 in the respective histone methyltransferase mutant strains. Shown are the ChIP-seq coverage tracks (normalized to 1x coverage with deeptools (115)) of one replicate per strain. As an example, the coverage of core chromosome 8 **(A)** and accessory chromosome 19 **(B)** is displayed. Based on the missing coverage, we confirm absence of H3K9me3 in the Δ*kmt1* and the Δ*k1/k6* strains and loss of H3K27me3 in the Δ*kmt6* and Δ*k1/k6* strains.
(PDF)

S4 Fig. Growth assay to compare *in vitro* fitness of mutant strains to Zt09. All strains were grown in liquid YMS medium at 18˚C and the OD_{600} was measured until the stationary phase was reached **(A)**. For each strain, two biological replicates were grown in technical triplicates

each. The growth of Δ*kmt1* and Δ*k1/k6* mutants was impaired compared to Zt09 and Δ*kmt6* but was restored in complemented strains. **(B)** We used the R package growthcurver [89] to calculate r-values for each growth curve. The values for Δ*kmt1* and Δ*k1/k6* were significantly lower compared to Zt09, but this was not the case in the complemented strains and Δ*kmt6* (Wilcoxon-rank sum test, * $p \leq 0.05$, ** $p \leq 0.01$).
(PDF)

S5 Fig. Assay to compare tolerance of Zt09 and mutants to different stress conditions including osmotic stress (NaCl and Sorbitol), oxidative stress (H2O2), genotoxic stress (MMS, actinomycin D), temperature stress (28˚C), cell wall stress (Congo Red), and nutrient starvation (H2O agar). We observed almost no differences between Zt09 and Δ*kmt6* strains, whereas Δ*kmt1* and Δ*k1/k6* mutants displayed decreased growth, as observed in the growth rate comparison.
(PDF)

S6 Fig. Stress assay to compare growth of deletion and respective complementation strains. **(A)** The Δ*kmt1* mutants showed overall decreased growth and were particularly sensitive to osmotic stress. These phenotypes were restored in the complemented strains. **(B)** Increased melanization at high temperatures, observed in the Δ*kmt6* mutants, was also reversed in the respective complementation strains.
(PDF)

S7 Fig. Plant infection phenotypes of Zt09 and mutant strains. We conducted three independent experiments, including 40 leaves per treatment and using at least two biological replicates per strain. Infection symptoms were evaluated and compared as the percentage of leaf area covered with pycnidia (asexual fruiting bodies) and necrotic lesions within the inoculated leaf areas by manual inspection as well as by automated image analysis of scanned leaves [90]. Symptoms in form of necrotic lesions and pycnidia were quantified after 21 days of infection either manually **(A)** and **(B)** or by automated image analysis of infected leaves **(C)** and **(D)**. Senescence on mock treated leaves was identified as necrosis by the automated image analysis and therefore all treatments, including mock treated leaves, show a high level of necrosis in this analysis. Furthermore, first appearance of symptoms was documented by daily screening of inoculated leaves **(E)** and **(F)**. If no symptoms in form of necrosis or pycnidia appeared during the screening period, no data is shown for those treatments. Virulence of both, Δ*kmt1* and Δ*k1/k6* strains was highly impaired. Δ*kmt6* strains were still able to produce necrosis as well as pycnidia, but the symptoms were reduced compared to Zt09. To evaluate if the decreased symptoms in Δ*kmt1* strains were due to the observed growth defects *in vitro*, we prolonged the infection time for one additional week **(G)** and **(H)**. Consistent with the results observed for 21 days post infection, the ability to infect was highly impaired and likely not correlated to the slower growth rate. Wilcoxon-rank sum test was performed to test for significant differences (* $p \leq 0.05$, ** $p \leq 0.01$, *** $p \leq 0.001$).
(PDF)

S8 Fig. Evolution experiments to monitor genome and chromosome stability during mitotic growth. **(A)** The short-term growth experiment over four weeks assessed stability of accessory chromosomes by screening individual clones in the populations for presence/absence of accessory chromosomes. Strains (Zt09, Δ*kmt1*, Δ*kmt6*, Δ*k1/k6*) were grown in triplicates for four weeks and 4% of the population were transferred to fresh medium every three to four days. After four weeks, single clones were isolated and screened for the presence/absence of accessory chromosomes by PCR. **(B)** A long-term growth experiment over six months was conducted to monitor genome stability in *Z. tritici* populations. Three replicate

populations per strain (Zt09, Δ*kmt1*, Δ*kmt6*) were grown in parallel exposed to the same growth conditions. 0.1% of the populations were transferred to fresh medium every three to four days. The genomes of the progenitor strains and all populations after six months of growth were sequenced to detect structural variation.
(PDF)

S9 Fig. Pulsed-field gel electrophoresis of mid-size chromosomes of Zt09 and Δ*kmt1* progenitor strains and the three single Δ*kmt1* clones originating from the evolved populations after 50 transfers. While there are no visible differences between the progenitor strains, all three single Δ*kmt1* clones exhibit different karyotypes. Chromosome size marker (M, in Mb) are *Saccharomyces cerevisiae* chromosomes (BioRad, Munich, Germany).
(PDF)

S10 Fig. Changes in chromosome structure detected in the evolved Δ*kmt1* clones Δ*kmt1*-50-1-1 and Δ*kmt1*-50-2-1. (A) Six duplicated regions were found in Δ*kmt1*-50-1-1, two each on chromosomes 1, 9 and 13. The breakpoints of the first duplicated sequence on chromosome 1 fused to the right telomeres of chromosome 13 (1*13) and 19 (1*19), the second duplication is a tandem duplication. While the right telomere of chromosome 19 fused to chromosome 1, the left arm including the centromere is deleted and *de novo* telomere formation occurred at the breakpoint. Chromosome 13 has two duplicated regions, one is a tandem duplication and one shows *de novo* telomere formation on both ends indicating a breakage of chromosome 13. The right telomere is fused to chromosome 1, the first breakpoint of the first duplicated region provides the new left telomere of the 1*13 chromosome. This breakpoint is located very close to the centromere. The left arm including the centromere forms a new, smaller chromosome 13_1, ending at the right breakpoint of the first duplicated region with *de novo* telomeres. Chromosome 9 did not fuse with another chromosome, but the structural variation rather led to the formation of two smaller chromosomes, both containing the duplicated sequences. The larger chromosome 9 (9_1), ends at the first breakpoint of the first duplicated region with *de novo* telomeres and ends at the breakpoint of the second duplicated region with *de novo* telomeres. The second duplicated region ends at the end of the chromosome where *de novo* telomere formation occurred as a result of chromosome breakage (~12 kb). In the smaller chromosome 9 (9_2), the two duplicated regions fused, deleting the entire sequence between the duplicated regions. **(B)** In the clone Δ*kmt1*-50-2-1, we detected four duplicated regions. While two are located on chromosome 9 and result in a very similar structural variation as described in (A), the other two are found on chromosome 1 and 8. One breakpoint of each duplicated region marks a fusion of the respective chromosomes, while the other one displays *de novo* telomere formation. As a result, three new chromosomes form. A new chromosome that represents a fusion of chromosomes 1 and 8 (1*8) and two chromosomes that are shorter version of chromosomes 1 (1_1) and 8 (8_1). The new, shorter versions both contain the centromeric sequence, while the fused chromosome does not contain any sequences of the original centromeres.
(PDF)

S11 Fig. Model for the formation of large structural rearrangements in the Δ*kmt1* mutants over time. 1: Replication stress at repeated sequences enriched with relocalized H3K27me3 promotes structural variation in form of deletion or duplication. **2:** Large segmental duplications arise during that process that are followed by chromosome breakage and new chromosomes are formed by adding *de novo* telomeric repeats at chromosomal breakpoints. While one of the chromosomal parts contains the original centromere, the other *de novo* chromosome forms a neocentromere. **3:** The duplicated sequences are targets for mitotic

recombination resulting in chromosome fusion. The chromosome is now dicentric. **4:** To stabilize the chromosome, one of the two centromeres is inactivated, either epigenetically or by deletion of the underlying sequence. **5:** Alternatively, the dicentric chromosome becomes unstable during mitosis and breaks between the two centromeres. The broken chromosome ends are repaired either by *de novo* telomere formation or fusion to a different chromosome, giving rise to new breakage-fusion-bridge cycles in following rounds of mitotic cell divisions. (PDF)

Acknowledgments

We thank all current and past members of the Environmental Genomics group for fruitful discussions and overall support.

Author Contributions

Conceptualization: Mareike Möller, Michael Freitag, Eva H. Stukenbrock.

Formal analysis: Mareike Möller, Jessica L. Soyer, Kristina M. Smith, Michael Freitag.

Funding acquisition: Michael Freitag, Eva H. Stukenbrock.

Investigation: Mareike Möller, Klaas Schotanus, Jessica L. Soyer, Janine Haueisen, Kathrin Happ, Maja Stralucke, Petra Happel, Lanelle R. Connolly, Michael Freitag.

Project administration: Michael Freitag, Eva H. Stukenbrock.

Resources: Jessica L. Soyer, Michael Freitag.

Supervision: Michael Freitag, Eva H. Stukenbrock.

Visualization: Mareike Möller.

Writing – original draft: Mareike Möller, Michael Freitag, Eva H. Stukenbrock.

Writing – review & editing: Mareike Möller, Klaas Schotanus, Jessica L. Soyer, Janine Haueisen, Michael Freitag, Eva H. Stukenbrock.

References

1. Goldberg AD, Allis CD, Bernstein E. Epigenetics: A Landscape Takes Shape. Cell. 2007; 128: 635–638. https://doi.org/10.1016/j.cell.2007.02.006 PMID: 17320500
2. Kornberg RD, Lorch Y. Chromatin structure and transcription. Annu Rev Cell Biol. 1992; 8: 563–587. https://doi.org/10.1146/annurev.cb.08.110192.003023 PMID: 1335747
3. Venkatesh S, Workman JL. Histone exchange, chromatin structure and the regulation of transcription. Nat Rev Mol Cell Biol. 2015; 16: 178–189. https://doi.org/10.1038/nrm3941 PMID: 25650798
4. Bannister AJ, Kouzarides T. Regulation of chromatin by histone modifications. Cell Res. 2011; 21: 381–395. https://doi.org/10.1038/cr.2011.22 PMID: 21321607
5. Harr JC, Gonzalez-Sandoval A, Gasser SM. Histones and histone modifications in perinuclear chromatin anchoring: from yeast to man. EMBO Rep. 2016; 17: e201541809.
6. Zimmer C, Fabre E. Principles of chromosomal organization: Lessons from yeast. J Cell Biol. 2011; 192: 723–733. https://doi.org/10.1083/jcb.201010058 PMID: 21383075
7. Freitag M. Histone Methylation by SET Domain Proteins in Fungi. Annu Rev Microbiol. 2017; 36: 413–439.
8. Rea S, Eisenhaber F, O'Carroll D, Strahl BD, Sun ZW, Schmid M, et al. Regulation of chromatin structure by site-specific histone H3 methyltransferases. Nature. 2000; 406: 593–599. https://doi.org/10.1038/35020506 PMID: 10949293
9. Allis CD, Berger SL, Cote J, Dent S, Jenuwien T, Kouzarides T, et al. New Nomenclature for Chromatin-Modifying Enzymes. Cell. 2007; 131(4):633–6. https://doi.org/10.1016/j.cell.2007.10.039 PMID: 18022353

10. Grewal SIS, Klar AJS. Chromosomal Inheritance of Epigentic States in Fission Yeast During Mitosis and Meiosis. Cell. 1996; 86: 95–101. PMID: 8689692
11. Tamaru H, Selker EU. A histone H3 methyltransferase controls DNA methylation in *Neurospora crassa*. Nature. 2001; 414: 277–83. https://doi.org/10.1038/35104508 PMID: 11713521
12. Mikkelsen TS, Ku M, Jaffe DB, Issac B, Lieberman E, Giannoukos G, et al. Genome-wide maps of chromatin state in pluripotent and lineage-committed cells. Nature. 2007; 448: 553–560. https://doi.org/10.1038/nature06008 PMID: 17603471
13. Zeller P, Padeken J, Van Schendel R, Kalck V, Tijsterman M, Gasser SM. Histone H3K9 methylation is dispensable for *Caenorhabditis elegans* development but suppresses RNA:DNA hybrid-associated repeat instability. Nat Genet. 2016; 48: 1385–1395. https://doi.org/10.1038/ng.3672 PMID: 27668659
14. Peters AHFM, O'Carroll D, Scherthan H, Mechtler K, Sauer S, Schöfer C, et al. Loss of the Suv39h histone methyltransferases impairs mammalian heterochromatin and genome stability. Cell. 2001; 107: 323–337. PMID: 11701123
15. Underwood CJ, Choi K, Lambing C, Zhao X, Serra H, Borges F, et al. Epigenetic activation of meiotic recombination near *Arabidopsis thaliana* centromeres via loss of H3K9me2 and non-CG DNA methylation. Genome Res. 2018; https://doi.org/10.1101/gr.227116.117 PMID: 29530927
16. Müller J, Hart CM, Francis NJ, Vargas ML, Sengupta A, Wild B, et al. Histone methyltransferase activity of a *Drosophila* Polycomb group repressor complex. Cell. 2002; 111: 197–208. PMID: 12408864
17. Goodrich J, Puangsomlee P, Martin M, Long D, Meyerowitz EM, Coupland G. A Polycomb-group gene regulates homeotic gene expression in *Arabidopsis*. Nature. 1997; 386: 44–51. https://doi.org/10.1038/386044a0 PMID: 9052779
18. Holec S, Berger F. Polycomb Group Complexes Mediate Developmental Transitions in Plants. Plant Physiol. 2012; 158: 35–43. https://doi.org/10.1104/pp.111.186445 PMID: 22086420
19. O'Carroll D, Erhardt S, Pagani M, Barton SC. The Polycomb -Group Gene Ezh2 Is Required for Early Mouse Development. Mol Cell Biol. 2001; 21: 4330–4336. https://doi.org/10.1128/MCB.21.13.4330-4336.2001 PMID: 11390661
20. Lee TI, Jenner RG, Boyer LA, Guenther MG, Levine SS, Kumar RM, et al. Control of Developmental Regulators by Polycomb in Human Embryonic Stem Cells. Cell. 2006; 125: 301–313. https://doi.org/10.1016/j.cell.2006.02.043 PMID: 16630818
21. Connolly LR, Smith KM, Freitag M. The *Fusarium graminearum* histone H3 K27 methyltransferase KMT6 regulates development and expression of secondary metabolite gene clusters. PLoS Genet.; 2013; 9: e1003916. https://doi.org/10.1371/journal.pgen.1003916 PMID: 24204317
22. Dumesic PA, Homer CM, Moresco JJ, Pack LR, Shanle EK, Coyle SM, et al. Product Binding Enforces the Genomic Specificity of a Yeast Polycomb Repressive Complex. Cell. 2015; 160: 204–218. https://doi.org/10.1016/j.cell.2014.11.039 PMID: 25533783
23. Jamieson K, Rountree MR, Lewis ZA, Stajich JE, Selker EU. Regional control of histone H3 lysine 27 methylation in *Neurospora*. Proc Natl Acad Sci U S A. 2013; 110: 6027–32. https://doi.org/10.1073/pnas.1303750110 PMID: 23530226
24. Holm K, Grabau D, Lövgren K, Aradottir S, Gruvberger-Saal S, Howlin J, et al. Global H3K27 trimethylation and EZH2 abundance in breast tumor subtypes. Mol Oncol. 2012; 6: 494–506. https://doi.org/10.1016/j.molonc.2012.06.002 PMID: 22766277
25. Ngollo M, Lebert A, Daures M, Judes G, Rifai K, Dubois L, et al. Global analysis of H3K27me3 as an epigenetic marker in prostate cancer progression. BMC Cancer. 2017; 17: 1–8. https://doi.org/10.1186/s12885-016-3022-6
26. Wei Y, Xia W, Zhang Z, Liu J, Wang H, Adsay N V, et al. Loss of trimethylation at lysine 27 of histone H3 is a predictor of poor outcome in breast, ovarian, and pancreatic cancers. Mol Carcinog.; 2008; 47: 701–706. https://doi.org/10.1002/mc.20413 PMID: 18176935
27. Basenko EY, Sasaki T, Ji L, Prybol CJ, Burckhardt RM, Schmitz RJ, et al. Genome-wide redistribution of H3K27me3 is linked to genotoxic stress and defective growth. Proc Natl Acad Sci U S A. 2015; 112 (46):E6339–48. https://doi.org/10.1073/pnas.1511377112 PMID: 26578794
28. Studt L, Rösler SM, Burkhardt I, Arndt B, Freitag M, Humpf H-U, et al. Knock-down of the methyltransferase Kmt6 relieves H3K27me3 and results in induction of cryptic and otherwise silent secondary metabolite gene clusters in *Fusarium fujikuroi*. Environ Microbiol. 2016; 18: 4037–4054. https://doi.org/10.1111/1462-2920.13427 PMID: 27348741
29. Chujo T, Scott B. Histone H3K9 and H3K27 methylation regulates fungal alkaloid biosynthesis in a fungal endophyte-plant symbiosis. Mol Microbiol. 2014; 92: 413–434. https://doi.org/10.1111/mmi.12567 PMID: 24571357
30. Galazka JM, Freitag M. Variability of chromosome structure in pathogenic fungi-of "ends and odds." Curr Opin Microbiol.; 2014; 20: 19–26. https://doi.org/10.1016/j.mib.2014.04.002 PMID: 24835423

31. Schotanus K, Soyer JL, Connolly LR, Grandaubert J, Happel P, Smith KM, et al. Histone modifications rather than the novel regional centromeres of *Zymoseptoria tritici* distinguish core and accessory chromosomes. Epigenetics Chromatin.; 2015; 8: 41. https://doi.org/10.1186/s13072-015-0033-5 PMID: 26430472

32. Hutchison CA, Chuang RY, Noskov VN, Assad-Garcia N, Deerinck TJ, Ellisman MH, et al. Design and synthesis of a minimal bacterial genome. Science. 2016; 351.aad6253 https://doi.org/10.1126/science.aad6253 PMID: 27013737

33. Covert SF. Supernumerary chromosomes in filamentous fungi. Curr Genet. 1998; 33: 311–319. PMID: 9618581

34. Möller M, Stukenbrock EH. Evolution and genome architecture in fungal plant pathogens. Nat Rev Microbiol. 2017; 15: 756–771. https://doi.org/10.1038/nrmicro.2017.76 PMID: 28781365

35. Ma L-J, van der Does HC, Borkovich K a, Coleman JJ, Daboussi M-J, Di Pietro A, et al. Comparative genomics reveals mobile pathogenicity chromosomes in *Fusarium*. Nature. 2010; 464: 367–373. https://doi.org/10.1038/nature08850 PMID: 20237561

36. Miao V, Covert S, VanEtten H. A fungal gene for antibiotic resistance on a dispensable ("B") chromosome. Science. 1991; 254: 1773–1776. PMID: 1763326

37. Van Dam P, Fokkens L, Ayukawa Y, Van Der Gragt M, Ter Horst A, Brankovics B, et al. A mobile pathogenicity chromosome in *Fusarium oxysporum* for infection of multiple cucurbit species. Sci Rep. 2017; 7: 1–15. https://doi.org/10.1038/s41598-016-0028-x

38. Johnson LJ, Johnson RD, Akamatsu H, Salamiah A, Otani H, Kohmoto K, et al. Spontaneous loss of a conditionally dispensable chromosome from the *Alternaria alternata* apple pathotype leads to loss of toxin production and pathogenicity. Curr Genet. 2001; 40: 65–72. PMID: 11570518

39. Habig M, Quade J, Stukenbrock EH. Forward genetics approach reveals host-genotype dependent importance of accessory chromosomes in the fungal wheat pathogen *Zymoseptoria tritici*. mBio. 2017; 8:e01919–17 https://doi.org/10.1128/mBio.01919-17 PMID: 29184021

40. Goodwin SB, Ben M'barek S, Dhillon B, Wittenberg AHJ, Crane CF, Hane JK, et al. Finished genome of the fungal wheat pathogen *Mycosphaerella graminicola* reveals dispensome structure, chromosome plasticity, and stealth pathogenesis. PLoS Genet. 2011; 7: e1002070. https://doi.org/10.1371/journal.pgen.1002070 PMID: 21695235

41. Kellner R, Bhattacharyya A, Poppe S, Hsu TY, Brem RB, Stukenbrock EH. Expression profiling of the wheat pathogen *Zymoseptoria tritici* reveals genomic patterns of transcription and host-specific regulatory programs. Genome Biol Evol. 2014; 6: 1353–1365. https://doi.org/10.1093/gbe/evu101 PMID: 24920004

42. Rudd JJ, Kanyuka K, Hassani-Pak K, Derbyshire M, Andongabo A, Devonshire J, et al. Transcriptome and metabolite profiling of the infection cycle of *Zymoseptoria tritici* on wheat reveals a biphasic interaction with plant immunity involving differential pathogen chromosomal contributions and a variation on the hemibiotrophic lifestyle def. Plant Physiol. 2015; 167: 1158–85. https://doi.org/10.1104/pp.114.255927 PMID: 25596183

43. Coleman JJ, Rounsley SD, Rodriguez-Carres M, Kuo A, Wasmann CC, Grimwood J, et al. The genome of *Nectria haematococca*: contribution of supernumerary chromosomes to gene expansion. PLoS Genet. 2009; 5: e1000618. https://doi.org/10.1371/journal.pgen.1000618 PMID: 19714214

44. Jin W, Lamb JC, Vega JM, Dawe RK, Birchler JA, Jiang J. Molecular and Functional Dissection of the Maize B Chromosome Centromere. Plant Cell. 2005; 17: 1412 LP–1423.

45. Vlaardingerbroek I, Beerens B, Schmidt SM, Cornelissen BJC, Rep M. Dispensable chromosomes in *Fusarium oxysporum* f. sp *lycopersici*. Mol Plant Pathol. 2016; 1–12.

46. Möller M, Habig M, Freitag M, Stukenbrock EH. Extraordinary Genome Instability and Widespread Chromosome Rearrangements During Vegetative Growth. Genetics. 2018; 210 no. 2: 517–529. https://doi.org/10.1534/genetics.118.301050 PMID: 30072376

47. Wittenberg AHJ, van der Lee T AJ, Ben M'barek S, Ware SB, Goodwin SB, Kilian A, et al. Meiosis drives extraordinary genome plasticity in the haploid fungal plant pathogen *Mycosphaerella graminicola*. PLoS One. 2009; 4: e5863. https://doi.org/10.1371/journal.pone.0005863 PMID: 19516898

48. Grandaubert J, Bhattacharyya A, Stukenbrock EH. RNA-seq Based Gene Annotation and Comparative Genomics of Four Fungal Grass Pathogens in the Genus *Zymoseptoria* Identify Novel Orphan Genes and Species-Specific Invasions of Transposable Elements. G3. 2015; 5: g3.115.017731–.

49. Bowler J, Scott E, Tailor R, Scalliet G, Ray J, Csukai M. New capabilities for *Mycosphaerella graminicola* research. Mol Plant Pathol. 2010; 11: 691–704. https://doi.org/10.1111/j.1364-3703.2010.00629.x PMID: 20696006

50. Mehrabi R, Mirzadi Gohari A, da Silva GF, Steinberg G, Kema GHJ, de Wit PJGM. Flexible gateway constructs for functional analyses of genes in plant pathogenic fungi. Fungal Genet Biol. 2015; 79: 186–192. https://doi.org/10.1016/j.fgb.2015.03.016 PMID: 26092806

51. Weber T, Blin K, Duddela S, Krug D, Kim HU, Bruccoleri R, et al. AntiSMASH 3.0-A comprehensive resource for the genome mining of biosynthetic gene clusters. Nucleic Acids Res. 2015; 43: W237–W243. https://doi.org/10.1093/nar/gkv437 PMID: 25948579

52. Klocko AD, Ormsby T, Galazka JM, Leggett NA, Uesaka M, Honda S, et al. Normal chromosome conformation depends on subtelomeric facultative heterochromatin in *Neurospora crassa*. Proc Natl Acad Sci. 2016; 113: 15048–15053. https://doi.org/10.1073/pnas.1615546113 PMID: 27856763

53. Harr JC, Luperchio TR, Wong X, Cohen E, Wheelan SJ, Reddy KL. Directed targeting of chromatin to the nuclear lamina is mediated by chromatin state and A-type lamins. J Cell Biol. 2015; 208: 33–52. https://doi.org/10.1083/jcb.201405110 PMID: 25559185

54. Heun P, Laroche T, Raghuraman MK, Gasser SM. The positioning and dynamics of origins of replication in the budding yeast nucleus. J Cell Biol. 2001; 152: 385–400. PMID: 11266454

55. Jørgensen HF, Azuara V, Amoils S, Spivakov M, Terry A, Nesterova T, et al. The impact of chromatin modifiers on the timing of locus replication in mouse embryonic stem cells. Genome Biol. 2007; 8: 1–13.

56. Buchenau P, Hodgson J, Strutt H, Arndt-Jovin DJ. The Distribution of Polycomb-Group Proteins During Cell Division and Development in *Drosophila* embryos: impact on models for silencing. Cell. 1998; 141: 469–481.

57. Messmer S, Franke A, Paro R. Analysis of the functional role of the Polycomb chromo domain in *Drosophila melanogaster*. Genes Dev. 1992; 6: 1241–1254. PMID: 1628830

58. Denholtz M, Bonora G, Chronis C, Splinter E, de Laat W, Ernst J, et al. Long-Range Chromatin Contacts in Embryonic Stem Cells Reveal a Role for Pluripotency Factors and Polycomb Proteins in Genome Organization. Cell Stem. 2013; 13: 602–616.

59. Banaei-Moghaddam AM, Schubert V, Kumke K, Weiβ O, Klemme S, Nagaki K, et al. Nondisjunction in Favor of a Chromosome: The Mechanism of Rye B Chromosome Drive during Pollen Mitosis. Plant Cell. 2012; 24: 4124–4134. https://doi.org/10.1105/tpc.112.105270 PMID: 23104833

60. Habig M, Kema G, Holtgrewe Stukenbrock E. Meiotic drive of female-inherited supernumerary chromosomes in a pathogenic fungus. eLife 2018; e40251 https://doi.org/10.7554/eLife.40251 PMID: 30543518

61. Fouché S, Plissonneau C, McDonald BA, Croll D. Meiosis Leads to Pervasive Copy-Number Variation and Distorted Inheritance of Accessory Chromosomes of the Wheat Pathogen *Zymoseptoria tritici*. Genome Biol Evol. 2018; 10: 1416–1429. https://doi.org/10.1093/gbe/evy100 PMID: 29850789

62. Peng JC, Karpen GH. Heterochromatic genome stability requires regulators of histone H3 K9 methylation. PLoS Genet. 2009; 5(3): e1000435 https://doi.org/10.1371/journal.pgen.1000435 PMID: 19325889

63. Kondo Y, Shen L, Ahmed S, Boumber Y, Sekido Y, Haddad BR, et al. Downregulation of histone H3 lysine 9 methyltransferase G9a induces centrosome disruption and chromosome instability in cancer cells. PLoS One. 2008; 3: e2037. https://doi.org/10.1371/journal.pone.0002037 PMID: 18446223

64. Voineagu I, Narayanan V, Lobachev KS, Mirkin SM. Replication stalling at unstable inverted repeats: Interplay between DNA hairpins and fork stabilizing proteins. Proc Natl Acad Sci USA. 2008; 105: 9936–9941. https://doi.org/10.1073/pnas.0804510105 PMID: 18632578

65. Khurana S, Oberdoerffer P. Replication stress: A lifetime of epigenetic change. Genes. 2015; 6: 858–877. https://doi.org/10.3390/genes6030858 PMID: 26378584

66. Allshire RC, Madhani HD. Ten principles of heterochromatin formation and function. Nat Rev Mol Cell Biol. 2017; 19: 229–244. https://doi.org/10.1038/nrm.2017.119 PMID: 29235574

67. Li PC, Petreaca RC, Jensen A, Yuan JP, Green MD, Forsburg SL. Replication Fork Stability Is Essential for the Maintenance of Centromere Integrity in the Absence of Heterochromatin. Cell Rep. 2013; 3: 638–645. https://doi.org/10.1016/j.celrep.2013.02.007 PMID: 23478021

68. Chiruvella KK, Liang Z, Wilson TE. Repair of double-strand breaks by end joining. Cold Spring Harb Perspect Biol. 2013; 5: a012757. https://doi.org/10.1101/cshperspect.a012757 PMID: 23637284

69. Pennaneach V, Putnam CD, Kolodner RD. Chromosome healing by de novo telomere addition in *Saccharomyces cerevisiae*. Mol Microbiol. 2006; 59: 1357–1368. https://doi.org/10.1111/j.1365-2958.2006.05026.x PMID: 16468981

70. Peters AHFM, Kubicek S, Mechtler K, O'Sullivan RJ, Derijck AAHA, Perez-Burgos L, et al. Partitioning and Plasticity of Repressive Histone Methylation States in Mammalian Chromatin. Mol Cell. 2003; 12: 1577–1589. PMID: 14690609

71. Deleris A, Stroud H, Bernatavichute Y, Johnson E, Klein G, Schubert D, et al. Loss of the DNA Methyltransferase MET1 Induces H3K9 Hypermethylation at PcG Target Genes and Redistribution of H3K27 Trimethylation to Transposons in *Arabidopsis thaliana*. PLoS Genet. 2012; 8(11): e1003062 https://doi.org/10.1371/journal.pgen.1003062 PMID: 23209430

72. Murphy PJ, Cipriany BR, Wallin CB, Ju CY, Szeto K, Hagarman JA, et al. Single-molecule analysis of combinatorial epigenomic states in normal and tumor cells. Proc Natl Acad Sci USA. 2013; 110: 7772–7777. https://doi.org/10.1073/pnas.1218495110 PMID: 23610441

73. Jamieson K, Wiles ET, McNaught KJ, Sidoli S, Leggett N, Shao Y, et al. Loss of HP1 causes depletion of H3K27me3 from facultative heterochromatin and gain of H3K27me2 at constitutive heterochromatin. Genome Res. 2016; 26: 97–107. https://doi.org/10.1101/gr.194555.115 PMID: 26537359

74. Cuomo CA, Güldener U, Xu J-R, Trail F, Turgeon BG, Di Pietro A, et al. The *Fusarium graminearum* genome reveals a link between localized polymorphism and pathogen specialization. Science. 2007; 317: 1400–1402. https://doi.org/10.1126/science.1143708 PMID: 17823352

75. Seidl MF, Cook DE, Thomma BPHJ. Chromatin Biology Impacts Adaptive Evolution of Filamentous Plant Pathogens. PLoS Pathog. 2016; 12: e1005920. https://doi.org/10.1371/journal.ppat.1005920 PMID: 27812218

76. Fokkens L, Shahi S, Connolly LR, Stam R, Schmidt SM, Smith KM, et al. The multi-speed genome of *Fusarium oxysporum* reveals association of histone modifications with sequence divergence and footprints of past horizontal chromosome transfer events. bioRxiv. 2018; https://doi.org/10.1101/465070

77. J Janevska S, Baumann L, Sieber CMK, Münsterkötter M, Ulrich J, Kämper J, et al. Elucidation of the Two H3K36me3 Histone Methyltransferases Set2 and Ash1 in *Fusarium fujikuroi* Unravels Their Different Chromosomal Targets and a Major Impact of Ash1 on Genome Stability. Genetics. 2018; 208: 153 LP–171

78. Linde CC, Zhan J, McDonald BA. Population Structure of *Mycosphaerella graminicola*: From Lesions to Continents. Phytopathology. 2002; 92: 946–955. https://doi.org/10.1094/PHYTO.2002.92.9.946 PMID: 18944019

79. Mehrabi R, Taga M, Kema GHJ. Electrophoretic and cytological karyotyping of the foliar wheat pathogen *Mycosphaerella graminicola* reveals many chromosomes with a large size range. Mycologia. 2007; 99: 868–76. PMID: 18333510

80. McDonald BA., Martinez JP. Chromosome length polymorphisms in a *Septoria tritici* population. Curr Genet. 1991; 19: 265–271.

81. Feschotte C, Pritham EJ. DNA Transposons and the Evolution of Eukaryotic Genomes. Annu Rev Genet. 2007; 41: 331–368. https://doi.org/10.1146/annurev.genet.40.110405.090448 PMID: 18076328

82. Barrón MG, Fiston-Lavier A-S, Petrov DA, González J. Population Genomics of Transposable Elements in *Drosophila*. Annu Rev Genet. 2014; 48: 561–581. https://doi.org/10.1146/annurev-genet-120213-092359 PMID: 25292358

83. Hedges DJ, Batzer MA. From the margins of the genome: Mobile elements shape primate evolution. BioEssays. 2005; 27: 785–794. https://doi.org/10.1002/bies.20268 PMID: 16015599

84. Poppe S, Dorsheimer L, Happel P, Stukenbrock EH. Rapidly Evolving Genes Are Key Players in Host Specialization and Virulence of the Fungal Wheat Pathogen *Zymoseptoria tritici* (*Mycosphaerella graminicola*). PLoS Pathog. 2015; 11(7): e1005055. https://doi.org/10.1371/journal.ppat.1005055 PMID: 26225424

85. Gibson DG, Young L, Chuang RY, Venter JC, Hutchison CA, Smith HO. Enzymatic assembly of DNA molecules up to several hundred kilobases. Nat Methods. 2009; 6: 343–345. https://doi.org/10.1038/nmeth.1318 PMID: 19363495

86. Zwiers LH, De Waard MA. Efficient *Agrobacterium tumefaciens*-mediated gene disruption in the phytopathogen Mycosphaerella graminicola. Curr Genet. 2001; 39: 388–393. PMID: 11525415

87. Southern EM. Detection of specific sequences among DNA fragments separated by gel electrophoresis. J Mol Biol. 1975; 98: 503–517. PMID: 1195397

88. Sambrock J, W. Russel D. Molecular Cloning: A Laboratory Manual(3rd edition). 2001

89. Sprouffske K, Wagner A. Growthcurver: an R package for obtaining interpretable metrics from microbial growth curves. BMC Bioinformatics. 2016; 17: 172. https://doi.org/10.1186/s12859-016-1016-7 PMID: 27094401

90. Stewart EL, Hagerty CH, Mikaberidze A, Mundt C, Zhong Z, McDonald BA. An improved method for measuring quantitative resistance to the wheat pathogen *Zymoseptoria tritici* using high throughput automated image analysis. Phytopathology. 2016; 106(7):782–788 https://doi.org/10.1094/PHYTO-01-16-0018-R PMID: 27050574

91. Soyer JL, Möller M, Schotanus K, Connolly LR, Galazka JM, Freitag M, et al. Chromatin analyses of *Zymoseptoria tritici*: Methods for chromatin immunoprecipitation followed by high-throughput sequencing (ChIP-seq). Fungal Genet Biol.; 2015; 79: 63–70. https://doi.org/10.1016/j.fgb.2015.03.006 PMID: 25857259

92. Allen GC, Flores-Vergara MA, Krasynanski S, Kumar S, Thompson WF. A modified protocol for rapid DNA isolation from plant tissues using cetyltrimethylammonium bromide. Nat Protoc. 2006; 1: 2320–2325. https://doi.org/10.1038/nprot.2006.384 PMID: 17406474

93. Bolger AM, Lohse M, Usadel B. Trimmomatic: A flexible trimmer for Illumina sequence data. Bioinformatics. 2014; 30: 2114–2120. https://doi.org/10.1093/bioinformatics/btu170 PMID: 24695404

94. Kim D, Langmead B, Salzberg SL. HISAT: a fast spliced aligner with low memory requirements. Nat Methods. 2015; 12: 357–60. https://doi.org/10.1038/nmeth.3317 PMID: 25751142

95. Langmead B, Salzberg SL. Fast gapped-read alignment with Bowtie 2. Nat Methods. 2012; 9: 357–359. https://doi.org/10.1038/nmeth.1923 PMID: 22388286

96. Li H. A statistical framework for SNP calling, mutation discovery, association mapping and population genetical parameter estimation from sequencing data. Bioinformatics. 2011; 27: 2987–2993. https://doi.org/10.1093/bioinformatics/btr509 PMID: 21903627

97. Heinz S, Benner C, Spann N, Bertolino E, Lin YC, Laslo P, et al. Simple Combinations of Lineage-Determining Transcription Factors Prime cis-Regulatory Elements Required for Macrophage and B Cell Identities. Mol Cell. 2010; 38: 576–589. https://doi.org/10.1016/j.molcel.2010.05.004 PMID: 20513432

98. Quinlan AR, Hall IM. BEDTools: a flexible suite of utilities for comparing genomic features. Bioinformatics. 2010; 26: 841–842. https://doi.org/10.1093/bioinformatics/btq033 PMID: 20110278

99. Trapnell C, Williams BA, Pertea G, Mortazavi A, Kwan G, van Baren MJ, et al. Transcript assembly and quantification by RNA-Seq reveals unannotated transcripts and isoform switching during cell differentiation. Nat Biotechnol. 2010; 28: 511–515. https://doi.org/10.1038/nbt.1621 PMID: 20436464

100. Anders S, Pyl PT, Huber W. HTSeq-A Python framework to work with high-throughput sequencing data. Bioinformatics. 2015; 31: 166–169. https://doi.org/10.1093/bioinformatics/btu638 PMID: 25260700

101. Ihaka R, Gentleman R. R: A Language for Data Analysis and Graphics. J Comput Graph Stat. 1996; 5: 299–314.

102. Love MI, Huber W, Anders S. Moderated estimation of fold change and dispersion for RNA-seq data with DESeq2. Genome Biol. 2014; 15: 1–21.

103. Alexa A, Rahnenführer J, Lengauer T. Improved scoring of functional groups from gene expression data by decorrelating GO graph structure. Bioinformatics. 2006; 22: 1600–1607. https://doi.org/10.1093/bioinformatics/btl140 PMID: 16606683

104. Chiang C, Layer RM, Faust GG, Lindberg MR, Rose DB, Garrison EP, et al. SpeedSeq: Ultra-fast personal genome analysis and interpretation. Nat Methods. 2015; 12: 966–968. https://doi.org/10.1038/nmeth.3505 PMID: 26258291

105. Layer RM, Chiang C, Quinlan AR, Hall IM. LUMPY: A probabilistic framework for structural variant discovery. Genome Biol. 2014; 15: 1–19.

106. Thorvaldsdóttir H, Robinson JT, Mesirov JP. Integrative Genomics Viewer (IGV): High-performance genomics data visualization and exploration. Brief Bioinform. 2013; 14: 178–192. https://doi.org/10.1093/bib/bbs017 PMID: 22517427

107. Ramírez F, Ryan DP, Grüning B, Bhardwaj V, Kilpert F, Richter AS, et al. deepTools2: a next generation web server for deep-sequencing data analysis. Nucleic Acids Res. 2016; 44: W160–W165. https://doi.org/10.1093/nar/gkw257 PMID: 27079975